2007-12

Structure and evolution of thermohaline staircases in tropical North Atlantic

Wall, Steven E.

Monterey, California. Naval Postgraduate School

NAVAL POSTGRADUATE SCHOOL

MONTEREY, CALIFORNIA

THESIS

STRUCTURE AND EVOLUTION OF THERMOHALINE STAIRCASES IN TROPICAL NORTH ATLANTIC

by

Steven Wall

December 2007

Thesis Advisor: Timour Radko
Second Reader: John Colosi

Approved for public release; distribution is unlimited

THIS PAGE INTENTIONALLY LEFT BLANK

REPORT DOCUMENTATION PAGE			Form Approved OMB No. 0704-0188
Public reporting burden for this collection of information is estimated to average 1 hour per response, including the time for reviewing instruction, searching existing data sources, gathering and maintaining the data needed, and completing and reviewing the collection of information. Send comments regarding this burden estimate or any other aspect of this collection of information, including suggestions for reducing this burden, to Washington headquarters Services, Directorate for Information Operations and Reports, 1215 Jefferson Davis Highway, Suite 1204, Arlington, VA 22202-4302, and to the Office of Management and Budget, Paperwork Reduction Project (0704-0188) Washington DC 20503.			
1. AGENCY USE ONLY *(Leave blank)*	**2. REPORT DATE** December 2007	**3. REPORT TYPE AND DATES COVERED** Master's Thesis	
4. TITLE AND SUBTITLE Structure and Evolution of Thermohaline Staircases in Tropical North Atlantic		**5. FUNDING NUMBERS**	
6. AUTHOR(S) Steven Edward Wall			
7. PERFORMING ORGANIZATION NAME(S) AND ADDRESS(ES) Naval Postgraduate School Monterey, CA 93943-5000		**8. PERFORMING ORGANIZATION REPORT NUMBER**	
9. SPONSORING /MONITORING AGENCY NAME(S) AND ADDRESS(ES) N/A		**10. SPONSORING/MONITORING AGENCY REPORT NUMBER**	
11. SUPPLEMENTARY NOTES The views expressed in this thesis are those of the author and do not reflect the official policy or position of the Department of Defense or the U.S. Government.			
12a. DISTRIBUTION / AVAILABILITY STATEMENT Approved for public release; distribution is unlimited		**12b. DISTRIBUTION CODE**	

13. ABSTRACT (maximum 200 words)

This study explores the dynamics of salt finger convection which occurs when warm, salty water overlies cool and fresh. Salt finger convection is generally observed in mid-latitude regions, particularly in the Atlantic Ocean and Mediterranean Sea, between the base of the mixed layer and the top of the intermediate water. Active salt fingering is characterized by the appearance of well mixed layers separated by thin high-gradient interfaces, known as thermohaline staircases. The data from the C-SALT, SFTRE and moored profiler experiments are analyzed to determine the origin of the thermohaline staircases and the mechanism for selection of the preferred layer thickness. Comparisons between these observations and models suggested by Radko are made. We use a combination of data analysis and analytical considerations to estimate the vertical heat/salt mixing rates and their dependencies on the large-scale environmental parameters. The three dimensional structure of these staircases and their evolution in time is explained by considering the secondary instabilities of a series of diffusive interfaces and the temporal and spatial structure of the high resolution data. Using a Parabolic Equation model we have investigated the influence of thermohaline staircases on acoustic propagation Also we experiment the sensitivity of the acoustic variations to changes in frequency and source depth.

14. SUBJECT TERMS Double diffusion, salt fingers, thermohaline staircases, acoustic propagation			**15. NUMBER OF PAGES** 104
			16. PRICE CODE
17. SECURITY CLASSIFICATION OF REPORT Unclassified	**18. SECURITY CLASSIFICATION OF THIS PAGE** Unclassified	**19. SECURITY CLASSIFICATION OF ABSTRACT** Unclassified	**20. LIMITATION OF ABSTRACT** UU

NSN 7540-01-280-5500 Standard Form 298 (Rev. 2-89)
Prescribed by ANSI Std. 239-18

THIS PAGE INTENTIONALLY LEFT BLANK

Approved for public release; distribution is unlimited

STRUCTURE AND EVOLUTION OF THERMOHALINE STAIRCASES IN TROPICAL NORTH ATLANTIC

Steven E. Wall
Lieutenant Commander, Royal Australian Navy
B.S., UNSW (ADFA), 1996
Graduate Diploma Meteorology, Bureau of Meteorology, 2001

Submitted in partial fulfillment of the
requirements for the degree of

MASTER OF SCIENCE IN PHYSICAL OCEANOGRAPHY

from the

NAVAL POSTGRADUATE SCHOOL
December 2007

Author: Steven Wall, RAN

Approved by: Timour Radko
Thesis Advisor

John Colosi
Second Reader

Mary Batteen
Chairman, Department of Physical Oceanography

THIS PAGE INTENTIONALLY LEFT BLANK

ABSTRACT

This study explores the dynamics of salt finger convection which occurs when warm, salty water overlies cool and fresh. Salt finger convection is generally observed in mid-latitude regions, particularly in the Atlantic Ocean and Mediterranean Sea, between the base of the mixed layer and the top of the intermediate water. Active salt fingering is characterized by the appearance of well mixed layers separated by thin high-gradient interfaces, known as thermohaline staircases. The data from the C-SALT, SFTRE and moored profiler experiments are analyzed to determine the origin of the thermohaline staircases and the mechanism for selection of the preferred layer thickness. Comparisons between these observations and models suggested by Radko are made. We use a combination of data analysis and analytical considerations to estimate the vertical heat/salt mixing rates and their dependencies on the large-scale environmental parameters. The three dimensional structure of these staircases and their evolution in time is explained by considering the secondary instabilities of a series of diffusive interfaces and the temporal and spatial structure of the high resolution data. Using a Parabolic Equation model we have investigated the influence of thermohaline staircases on acoustic propagation. Also we experiment the sensitivity of the acoustic variations to changes in frequency and source depth.

THIS PAGE INTENTIONALLY LEFT BLANK

TABLE OF CONTENTS

THIS PAGE INTENTIONALLY LEFT BLANK

LIST OF FIGURES

THIS PAGE INTENTIONALLY LEFT BLANK

LIST OF TABLES

ACKNOWLEDGMENTS

I would especially like to thank my advisor, Timour Radko, for his belief and patience in this project. He is a brilliant man and an extraordinarily gifted teacher. I would also like to thank John Colosi for sparking my interest in a field that I did not enjoy in the past. I would also like to thank Mike Cook, who will mostly likely have peace as I will not be bugging him for MATLAB assistance anymore.

Many thanks also to Prof Mary Batteen and all the lecturers and assistants in the Oceanography department at NPS (especially Jamie MacMahan and Tom Herbers) and selected ones from the Meteorology department (Tom Murphree and Ken Davidson).

I would also like to show my appreciation to Ray Schmitt and John Toole from WHOI for use of the data they collected and helpful insights and encouragement.

Cheers to the many friends and colleagues that have made this process easier (Ana, Ivo, Alban, Katherine, Christi, Erin, Frank and the Aussie contingent especially).

Most importantly I would like to thank my wife, Amanda, and my two children, Lachlan and Danae, for the support and love they have given me over this time. The time spent on this project impacted on them the most.

THIS PAGE INTENTIONALLY LEFT BLANK

I. INTRODUCTION

'Thermohaline staircases' have attracted considerable interest since continuous profiling of the water column showed fine-scale structures with stepped patterns of temperature and salinity. This study is focused on observational data from the western tropical North Atlantic (a noted area for the formation of the staircases). The data analysis is supplemented by theoretical considerations in an attempt to show that these features have a considerable impact on ocean mixing and acoustic performance and therefore have an impact operationally on the Navy and its interests.

A. HISTORY

In 1857, W.S. Jevons in Sydney, Australia observed long, narrow convection cells when warm, sugary water was placed over cool, fresh water. He correctly attributed this to the different diffusivities of sugar and heat (Jevons 1857), but misinterpreted the detailed physics. Notably, some of his work motivated Rayleigh's famous derivation for the frequency of an internal wave in a stratified fluid (Rayleigh 1883). This field remained largely unexplored until well into the next century.

It was not until the 'perpetual salt fountain' (Stommel et. al. 1955) that the idea surfaced again and double-diffusion was 're-discovered'. Theories developed by Melvin Stern, motivated by the salt fountain concept, coupled with subsequent laboratory experiments for the first time revealed the detailed physics of double-diffusive convection

(Stern, 1960). The structures resulting from double diffusive instability were shown to be long, narrow filaments, like those shown in Figure 1 (below), leading to the term 'salt fingers'. The scale of the figure is of the order of 30 centimeters for both the horizontal and vertical axes.

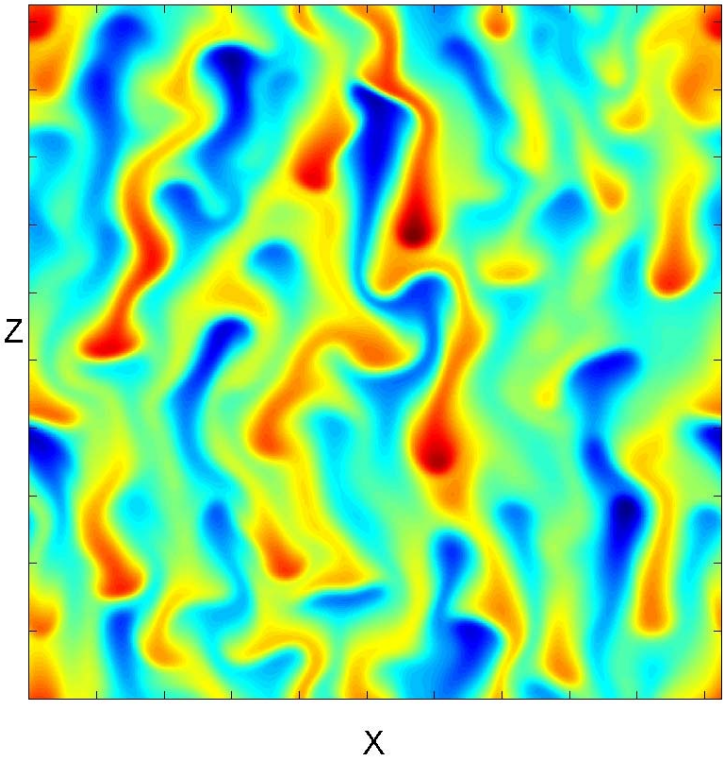

Figure 1. Numerical simulation of Salt Fingers, red indicates high salinity, (From Radko 2007)

Stern's (1960) analysis was soon followed by Turner's (1965, 1967) insightful laboratory experiments. A key step in quantifying the vertical heat and salt fluxes driven by double diffusion was associated with the so-called 4/3 flux laws. These flux laws form the basis for much of the work in this field to date.

One of the most striking features of double diffusive convection is their signature, apparent by a series of mixed layers separated by sharp interfaces. The discovery of these 'thermohaline staircases' by Tait and Howe (1968) further stimulated interest in double diffusion and its large-scale consequences in the ocean. Concurrent laboratory experiments attempted to explain the physics of double diffusive layering and specify the conditions leading to their formation. Some examples of thermohaline staircases from around the world are shown in Figure 2.

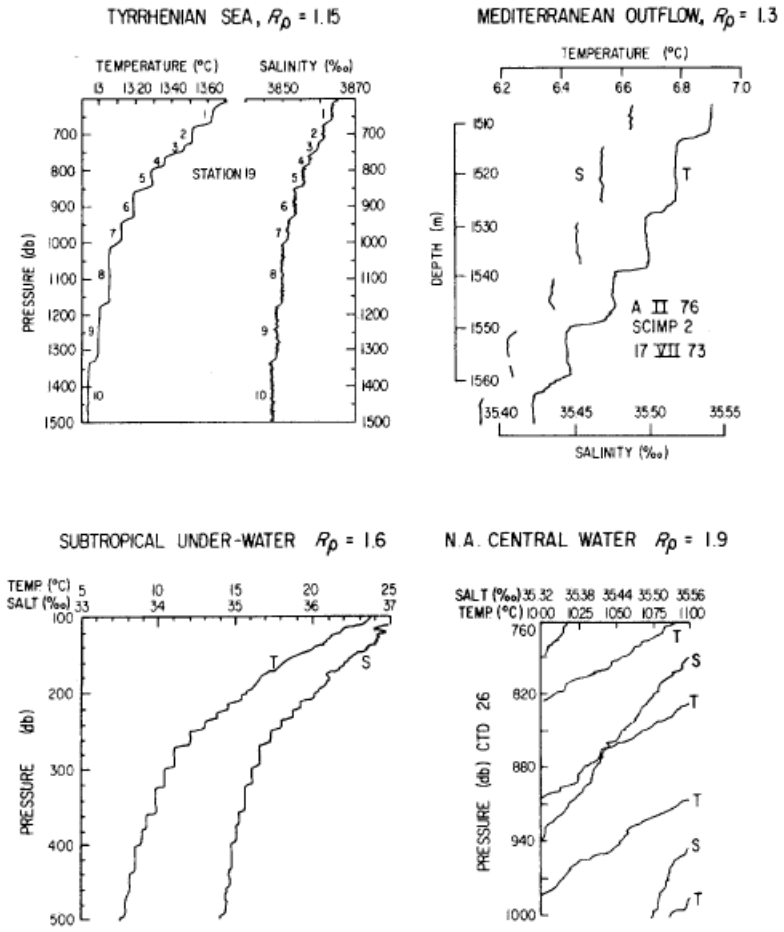

Figure 2. Observations of staircases. (From Schmitt 2003)

The abundance opf thermohaline staircases in the oceans, combined with the elevated temperature and salt fluxes in staircases (Schmitt 2005), suggest that these features can play a major role in ocean mixing and affect the large-scale circulation pattern.

Some observations, including the Carribean-Sheets and Layers Transect(C-SALT, Schmitt et. al., 1987) have shown that the interfaces are not as sharp as theorized and the fluxes may not be adequately estimated by the extrapolation of the laboratory-derived 4/3 flux laws. This uncertainty with regard to double-diffusive transport has lead to a large number of experiments, observations and numerical simulations in an attempt to rationalize the flux laws proposed by Turner. The exact magnitude of the temperature and salinity fluxes by double-diffusive processes is still a subject of scientific debate. As stated by Ruddick and Garret (2003) 'Salt fingers are effectively not quantified, and we cannot say exactly why not.'

B. DYNAMICS OF DOUBLE DIFFUSION

When the density of a stratified fluid at rest is decreasing with height, conventional wisdom dictates that the fluid is stable. This is true except when the stratification involves two (or more) constituents with differing molecular diffusivities. This sets up instabilities generated by the faster diffusion of one component over the other. These processes are known as multi-component convection (Turner, 1985) and lead to efficient mixing in the vertical plane.

As opposed to turbulent mixing, which increases potential energy and dissipates kinetic energy, multi-component convection processes decrease the potential energy of the system stored in the unstable gradient of the destabilizing constituent.

When this involves only two constituents, the process is known as double diffusion. In the ocean the two components are temperature and salt with kinematic diffusivities of ~1.4x 10^{-7} m^2/s and ~1.1x 10^{-9} m^2/s respectively.

Double diffusion in the ocean can take one of two forms; salt fingers and diffusive convection.

1. Salt Fingers

Salt fingering can occur when warm, salty water lies above cool, fresh water (see Figure 2a). In the ocean this configuration is common. Salt fingers are often observed in the sub-tropics, where high evaporation causes high salinity at the surface (for example the tropical North Atlantic); and near outflows of semi-enclosed seas that have greater evaporation than the surrounding open ocean (for example the Atlantic Ocean near Mediterranean Sea outflow region). The temperature stratification overcompensates for the unstable salinity stratification, and the system is statically stable.

The physics of salt fingering can be illustrated by the following argument. Consider a two layer system with the above characteristics (warm and salty over cool and fresh). If a fluid parcel is displaced from the top layer into the bottom layer it would normally return after executing a

number of oscillations in the vertical. In this system, however, when the parcel is displaced downward it loses heat to its surroundings and becomes heavier (whilst maintaining its original salinity due to the lower diffusivity and keeps moving down. This process can also happen in reverse, with a parcel displaced upwards becoming warmer and lighter (less salty). The motion takes the form in narrow, vertically elongated structures (as shown in Figure 1) giving rise to the term 'salt fingers'. This process is very efficient at transferring properties between the two layers.

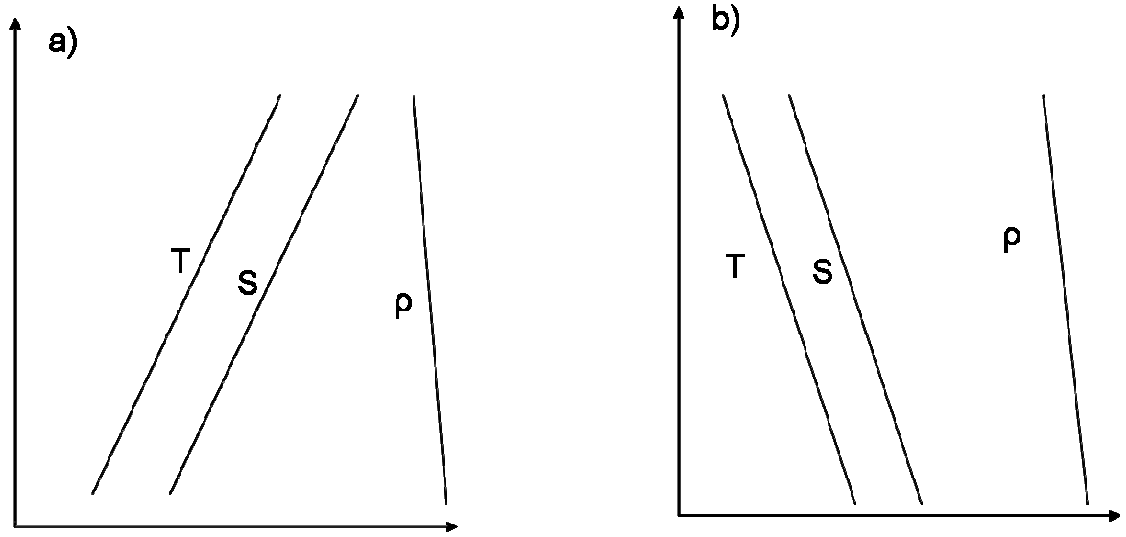

Figure 3. Simplified diagram of ocean double diffusive regimes. a) Salt Finger Regime b) Diffusive Convection Regime (From Clayson and Kantha 2000)

2. Diffusive Convection

Diffusive convection can occur when cold, fresh water lies above warm, salty water (Figure 2b). This occurs in the ocean in the Arctic and Antarctic where ice melt and surface cooling forms cooler, fresher water above subsurface waters and where there is a source of thermal heating and salts in the deep ocean. The salinity stratification

overcompensates for the unstable temperature stratification, and the system is statically stable.

This study is focused on the salt finger situation, and a similar analysis of the diffusive convection was presented by Wilson (2007).

C. THEORETICAL BACKGROUND

The intensity of salt fingering is controlled by the density ratio, which, for the salt finger case, is defined as:

$$R_\rho = \alpha \Delta T / \beta \Delta S \tag{1}$$

where:

$$\alpha = -\frac{1}{\rho}\left(\frac{\partial \rho}{\partial T^*}\right)_{S^*,P^*}$$
$$\beta = \frac{1}{\rho}\left(\frac{\partial \rho}{\partial S^*}\right)_{T^*,P^*} \tag{2}$$

α is the coefficient of thermal expansion at constant pressure and salinity and β is the coefficient of saline expansion at constant pressure and temperature.

When R_ρ < 1 the density gradient is unstable and will overturn. The upper limit for the formation of salt fingers, is set by the ratio of thermal (κ_T) and salt (κ_S) kinematic diffusivities (also known as the Lewis Number, κ_T/κ_S): $R_\rho < \kappa_T/\kappa_S \sim 100$.

The growth rate of the fingers does not become significantly large unless R_ρ is of the O (1). Schmitt (1979) found that the growth rate of the fingers becomes O ($N/2\pi$) (N is Buoyancy Frequency) when R_ρ < 2. The figure below indicates the dependence of growth rate on density

ratio and also identifies the density ratio in some of the major areas where salt fingers and thermohaline staircases have been observed.

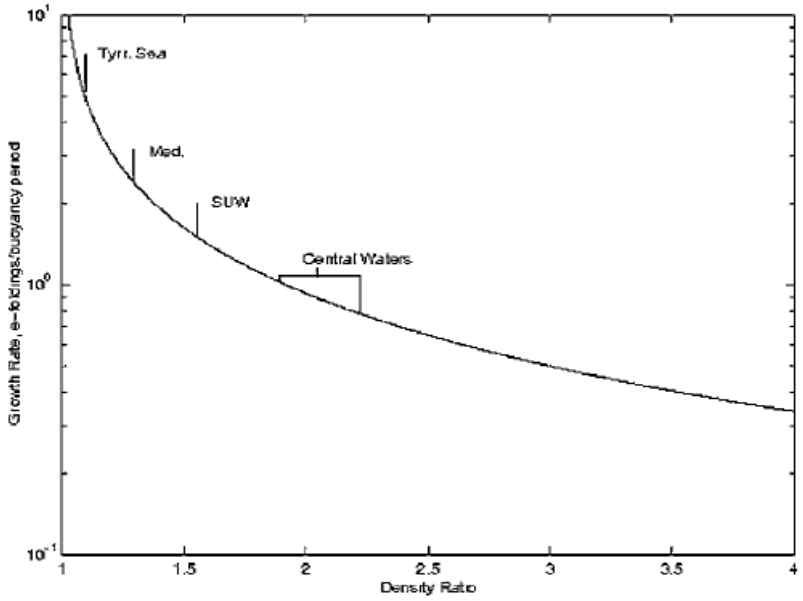

Figure 4. Growth rate of salt fingers as a function of Density ratio. (From Schmitt 2003)

For the growth rate of the fingers to compete with mechanical turbulence caused by oceanic shear and strain, the density ratio must remain low. (Stuebe 2005)

Another important parameter is the flux ratio, γ. γ is defined as $\alpha F_T/\beta F_S$ (where F_T and F_S are the molecular fluxes of heat and salinity respectively) and must be less than one to satisfy energy requirements, namely the net transport of density 'up gradient'. The dependence of the flux ratio on density ratio is very important in the formation of the staircases and is discussed in further detail below.

D. FORMATION OF STAIRCASES

One of the striking features of the double diffusive process is the formation of a series of homogeneous, convecting layers separated by thin, sharp interfaces (thermohaline steps or staircases). An example is shown in Figure 5 (below).

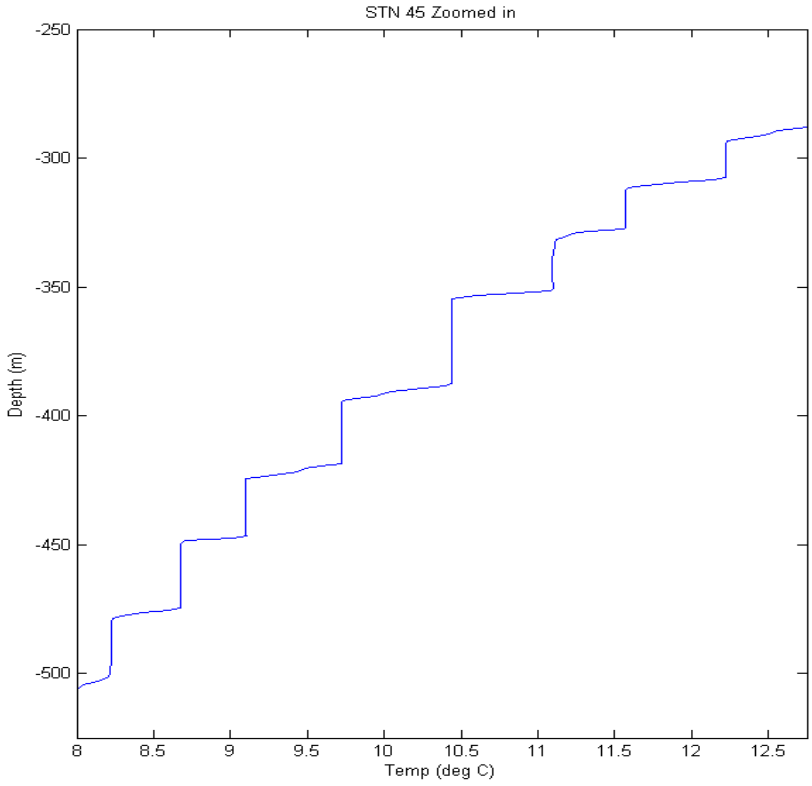

Figure 5. Thermohaline staircases (C-SALT STN 46)

It has been shown from laboratory experiments that when a stable linear temperature gradient is subjected to an imposed salinity flux at the vertical boundaries the structures as described above can form (Turner 1973). Numerical simulations have also shown that the spontaneous forming of layers occurs when the density ratio is sufficiently small O(1) (Radko 2003).

Various theories have been forwarded for the formation of the staircases. These include:

i) Thermohaline intrusions. (Merryfield 2000),

ii) Collective instability (Stern 1960),

iii) Metastable equilibria (Stern and Turner 1969),

iv) Negative density diffusion (Schmitt 1994),

v) Instability of the flux-gradient laws (Radko 2003)

The theory accepted in this analysis is the collective instability of the gradient flux laws, discussed in detail in Radko (2003) in which layering is attributed to the dependence of the flux ratio on the density ratio. An example of the numerical simulation showing staircase formation is shown below.

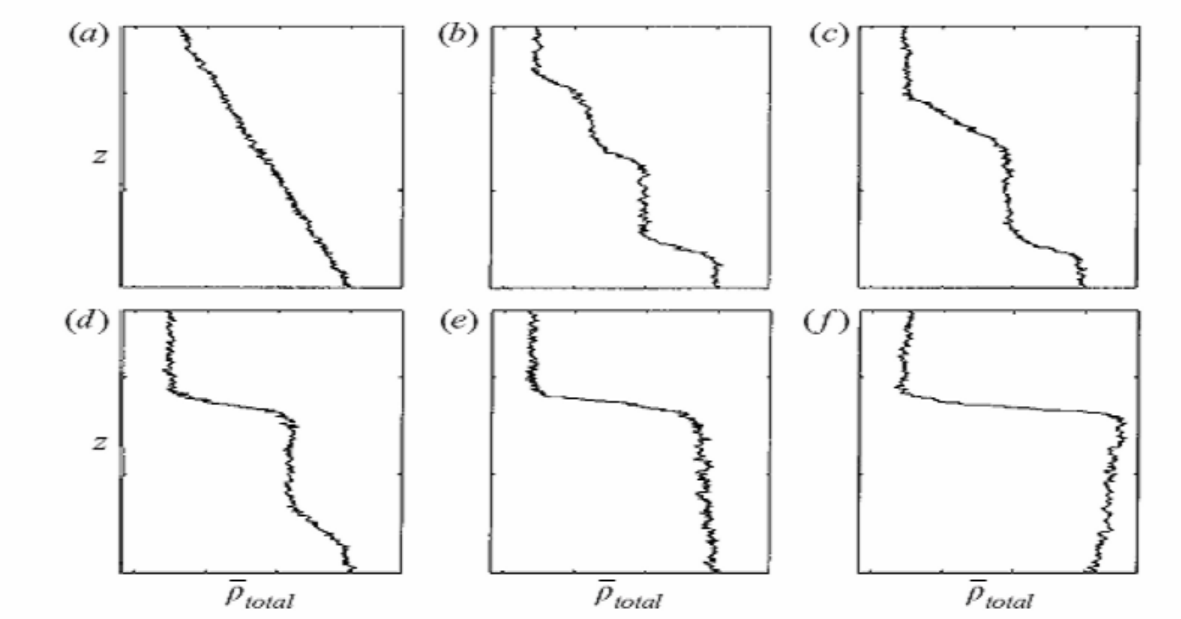

Figure 6. Numerical simulation of staircase formation. (From Radko 2003)

1. Turner's 4/3 Flux Laws

Turner (1965) hypothesized that if steps are sufficiently large ($H \to \infty$), the dependence of the vertical fluxes of temperature and salinity (F_T and F_S) on H would be weak, and therefore fluxes would be determined by the temperature and salinity variations $(\Delta T, \Delta S)$ across the step:

$$\begin{aligned} F_T &= F_T(\alpha\Delta T, \beta\Delta S, \kappa_T, \kappa_S, \upsilon, g) = F_T(\alpha\Delta T, R_\rho, \kappa_T, g, \tau, P_r) \\ F_S &= F_S(\alpha\Delta T, \beta\Delta S, \kappa_T, \kappa_S, \upsilon, g) = F_T(\alpha\Delta T, R_\rho, \kappa_T, g, \tau, P_r) \end{aligned} \quad (3)$$

where υ is viscosity, τ is the diffusivity ratio and P_r is the Prandtl number $\left(\frac{\upsilon}{\kappa_T}\right)$.

Using the dimensional argument that a non-dimensional number can depend only on other non-dimensional numbers, Turner then suggested that the so-called Nusselt number,

$$Nu = \frac{F_T}{\kappa_T \frac{\Delta T}{H}}, \quad (4)$$

measuring the fluxes would be related to the Raleigh number, measuring boundary forcing:

$$R_a = \frac{g\alpha\Delta T H^3}{\kappa_T \upsilon}. \quad (5)$$

$$Nu = C(R_a)^n \Rightarrow \alpha F_T = \left(\frac{g\alpha\Delta T H^3}{\kappa_T \upsilon}\right)^n * \kappa_T \frac{\alpha\Delta T}{H} \quad (6)$$

Turner hypothesized that there should be no dependence on H, therefore n=1/3. The resulting expressions for F_T and F_S are known as the "4/3 Flux Laws".

Whilst there is general agreement in the literature that double diffusive temperature and salinity fluxes are controlled by the density ratio, there is still considerable

uncertainty with regard to the extrapolation of the lab-based flux estimations to observed values in thermohaline staircases.

On the basis of dimensional considerations and laboratory experimentation, it could also be argued that for given molecular properties, the flux ratio, γ is a function of R_ρ. This was further explored by Radko (2003) and the figure below represents the dependence of both the flux ratio and Nusselt number on density ratio.

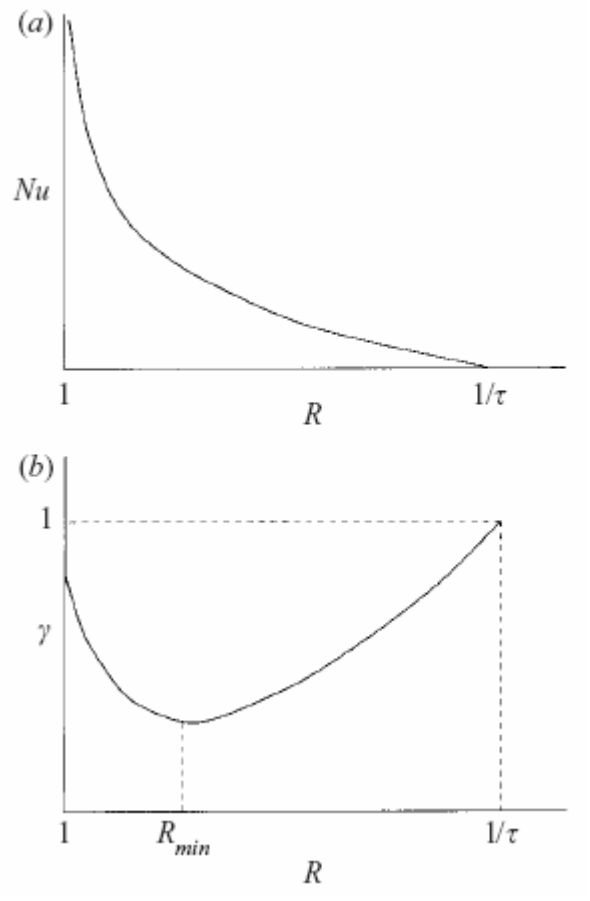

Figure 7. Dependence of Flux Ratio and Nusselt number on density ratio. (From Radko 2003)

The aforementioned models offer simple conceptual explanations for the dependences of vertical fluxes on temperature and salinity variations across the steps $(\Delta T, \Delta S)$. A separate question arises as to what controls ΔT, ΔS and ΔH in the oceanic staircases. Kelley (1988) and Radko (2005) suggest that these step characteristics are controlled by a layer-merging process. This merging process can be defined as the coalescence of thin, adjacent layers to form new, thicker layers, and their eventual equilibration (Wilson 2007). The merging process is explored further in Chapter III.

E. DISTRIBUTION OF STAIRCASES

There are several regions of the world's oceans with the potential for double-diffusion. One of the measures of the propensity for double diffusion is given by the so called Turner angle. The Turner Angle is defined as $Tu = \arctan(R_\rho) - 45$.

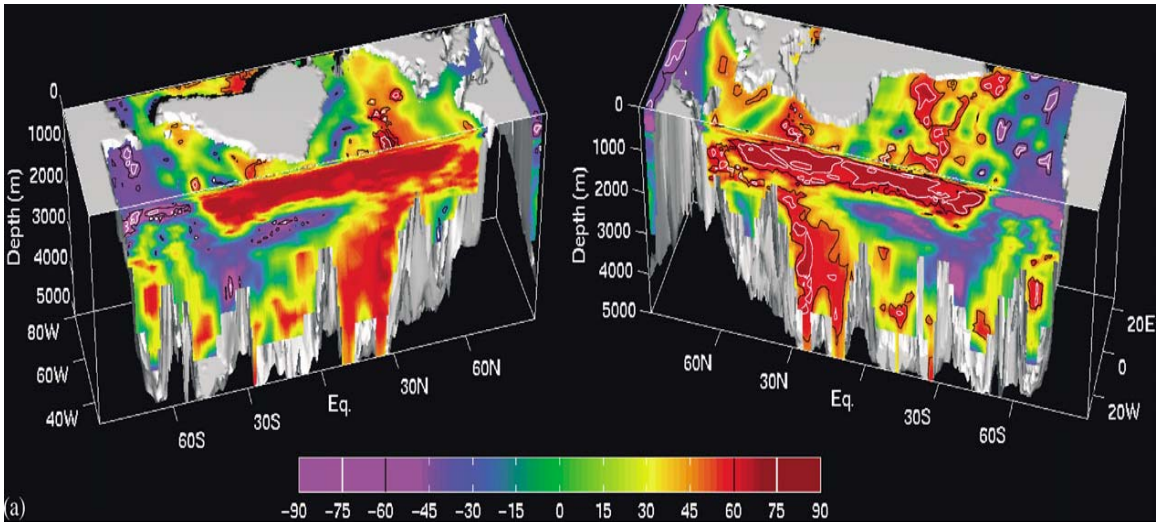

Figure 8. Turner Angle Values in the Atlantic Ocean (red areas are favorable for salt fingering) (From You 2002).

Figure 8 (above) indicates the distribution of *Tu* in the Atlantic Ocean. Red areas indicate favorable density ratios for salt finger formation and purple indicates areas favorable for diffusive convection, suggesting that much of the Atlantic is strongly unstable with regard to double-diffusion, salt-fingering in particular.

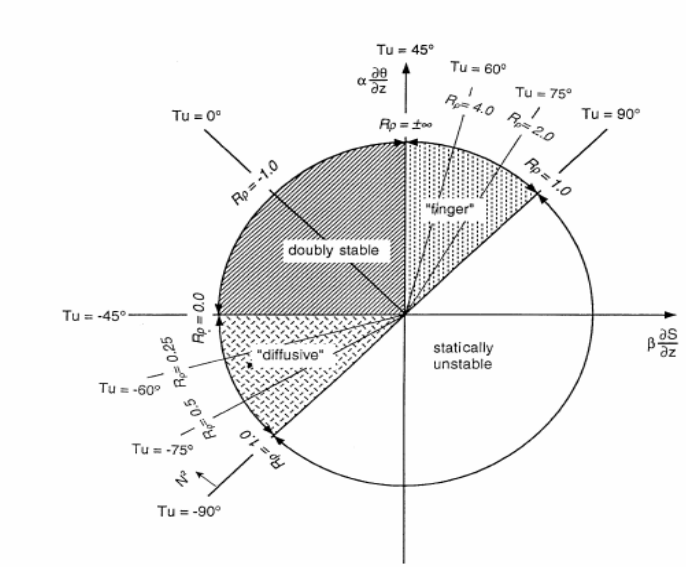

Figure 9. Turner Angle definition (From You 2002).

However, the density ratio must be less than 2 (close to 1.7) to allow the salt fingering process to form thermohaline staircases. The western tropical North Atlantic is an area with a low density ratio and and is therefore particularly susceptible to salt finger formation.

The salt-finger favorable conditions are due to Subtropical Under Water (salinity maximum) flowing west and meeting Antarctic Intermediate Water (salinity minimum) flowing north and this is highlighted in Figure 10 (below). This creates a region of several hundred meters (~200 to

700m) deep, covering an area of several thousand square kilometers, with high vertical temperature and salinity gradients and low density ratios – features that ultimately cause the formation of thermohaline staircases.

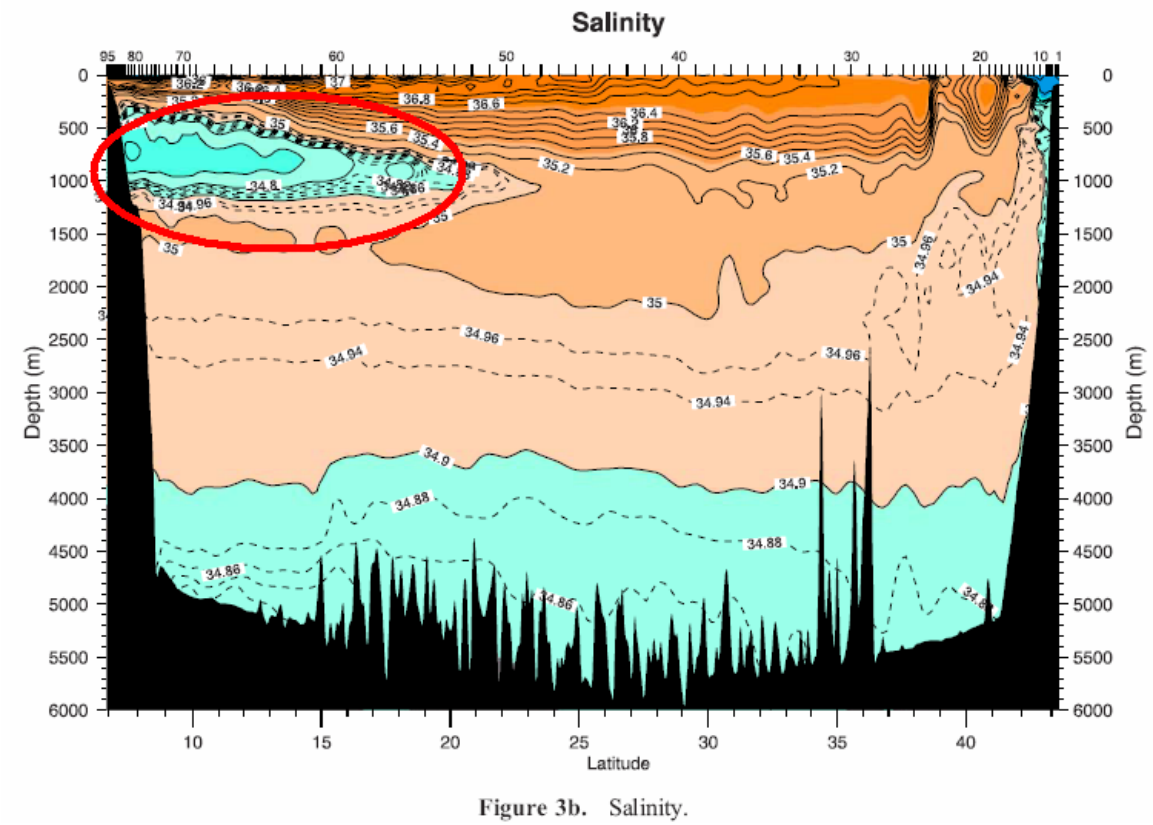

Figure 10. Cross section of the salinity of Atlantic along 52W (the salinity minimum due to the Antarctic Intermediate Water around 700m is highlighted) (From Hall et. al. 2004)

THIS PAGE INTENTIONALLY LEFT BLANK

II. GENERAL PROPERTIES OF THERMOHALINE STAIRCASES

A. DATA USED IN THIS STUDY

The data used in this study were collected in the western Tropical North Atlantic in a series of different experiments: C-SALT (1985) and the moored profiler (2001) (data from the moored profiler are used in Chapter III).

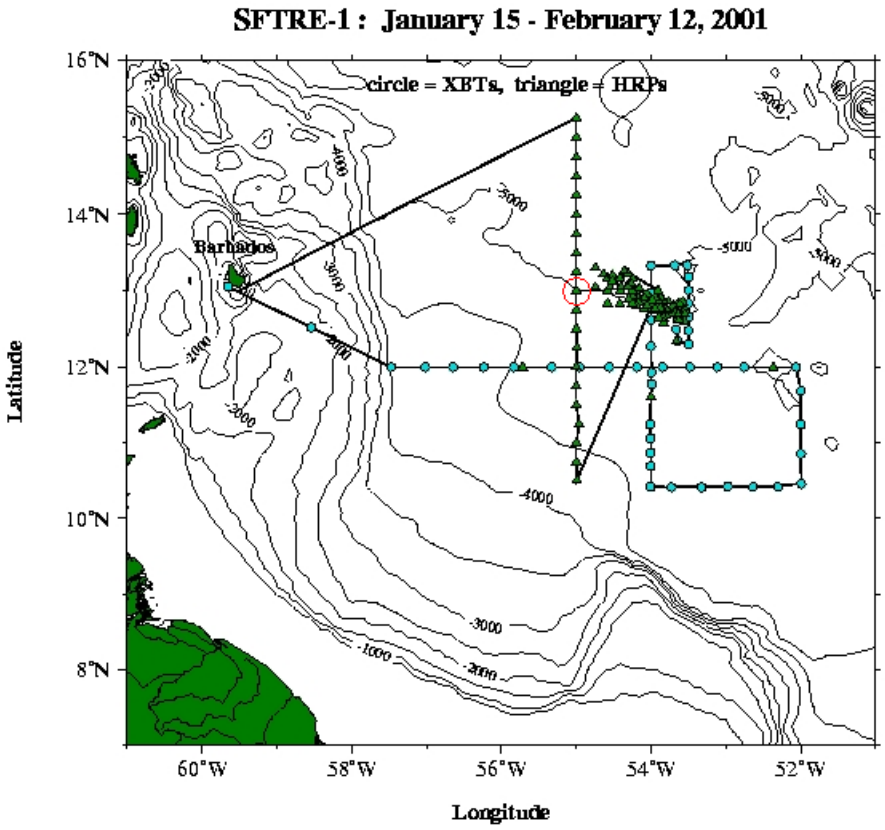

Figure 11. Location of moored profiler (red circle) and SFTRE profiles. (From Stuebe 2005)

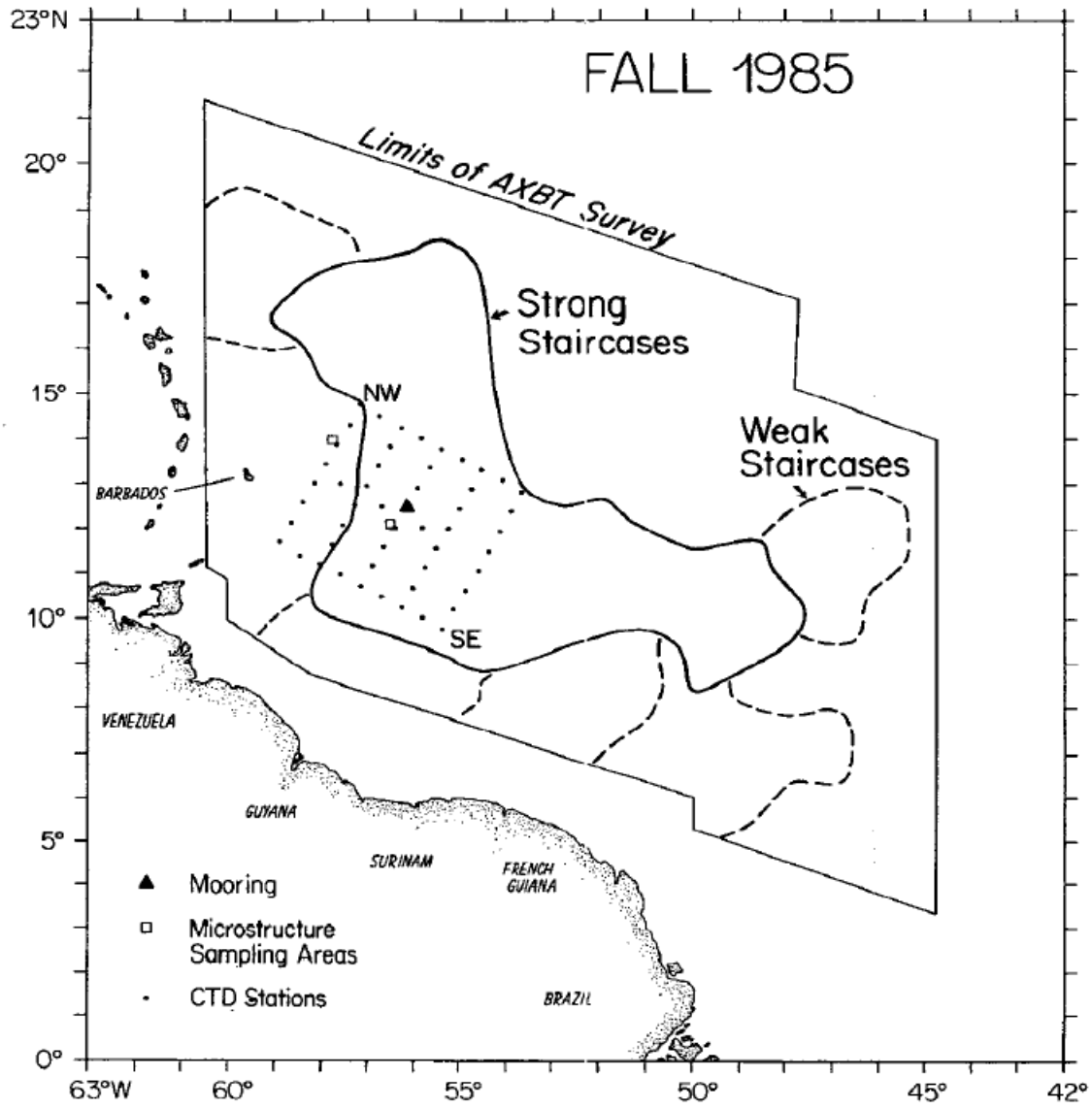

Figure 12. C-SALT observation area (From Schmitt, et al., 1987)

Of the 314 Conductivity Temperature and Depth (CTD) profiles that were conducted during C-SALT, 14 did not have well-defined thermohaline staircases.

Group	STNs	Dates	No. with Staircases	No. with no Staircases
1	1-14	30 Oct-1 Nov	9	4
2	15-32	2-5 Nov	18	0
3	33-48	6-9 Nov	15	2
4	49-52Y.014	10-11 Nov	25	0
5	52Y.016-54	11 Nov	21	0
6	56-58	17-18 Nov	25	8
7	60-64	20-21 Nov	25	0
8	65-69	22 Nov	34	0
9	70X.000-75X.004	23 Nov	27	0
10	75X.006-80X.004	24 Nov	30	0
11	80X.006-80X.066	25 Nov	31	0
12	81-86	26-27 Nov	15	0
13	87x.000-95	28-29 Nov	25	0

Table 1. Grouped data from C-SALT profiles.

To simply the analysis, all the data were separated in 13 groups ,based on the geographic location of measurements (Table 1).

The profiles were run through a MATLAB program that identified the centers of the steps and also the edges of the interfaces as shown below.

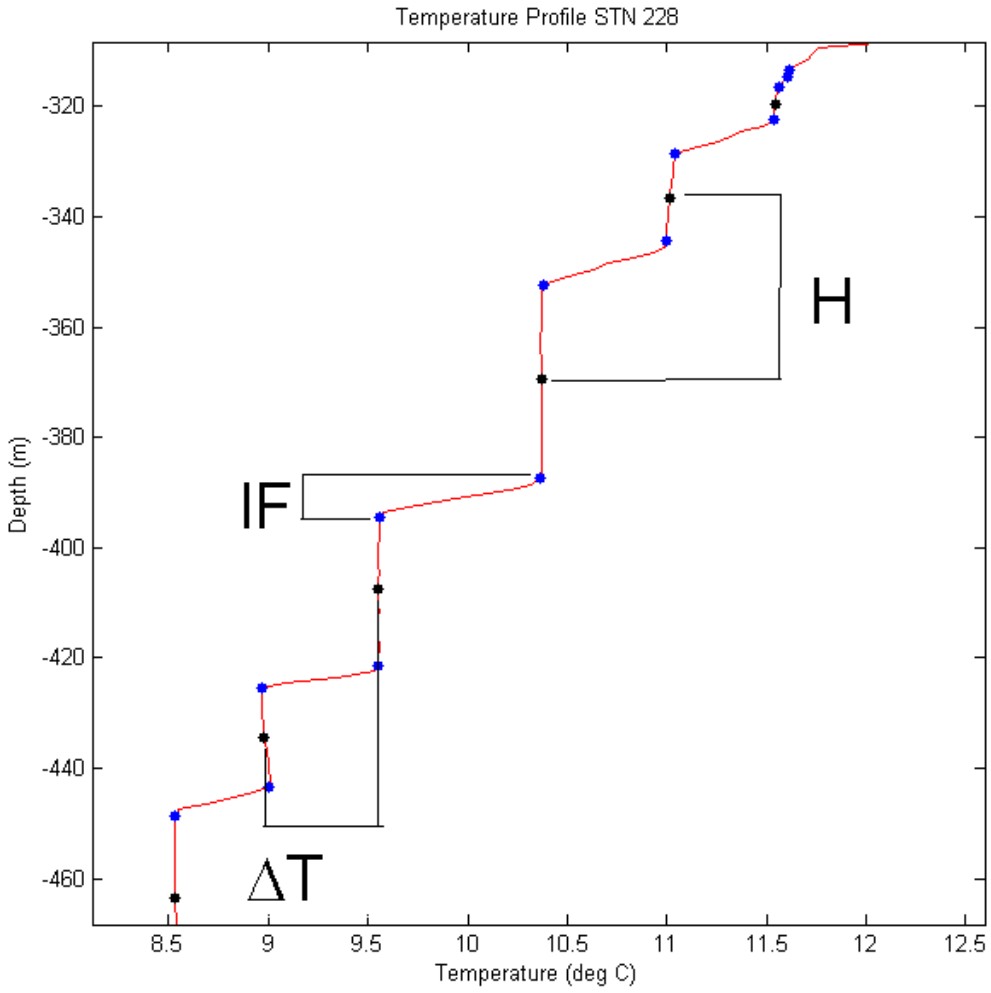

Figure 13. Temperature profile showing centers of steps (black), interfaces (blue) and definitions of step height and interfaces

Some of the basic statistics are tabulated below. Start depth is the average depth at which staircase type features are first identified and end depth is where the features are no longer recognizable. The number of steps is the average number of nearly homogenous layers and the step height is the average distance between two vertical means. The interface height is the average distance between the end

of one layer and the begging of another. ΔT and ΔS is the average difference between temperature and salinity values of the vertical means respectively.

Group	**Start Depth**	**End Depth**	**No.of steps**	**Step Height**	**Interface height**	**ΔT**	**ΔS**
1	310	440	6	12.7	5.3	0.28	0.04
2	270	530	11	19.1	5.0	0.40	0.06
3	275	485	10	17.2	5.3	0.36	0.05
4	230	440	11	16.2	5.6	0.44	0.07
5	245	485	13	18.5	5.6	0.46	0.07
6	335	410	5	12.9	5.3	0.23	0.04
7	295	585	12	18.3	5.3	0.31	0.04
8	270	550	13	18.3	5.2	0.40	0.06
9	290	565	12	17.7	4.8	0.37	0.05
10	260	560	12	17.5	5.1	0.38	0.06
11	255	540	12	18.2	5.0	0.41	0.06
12	325	525	8	13.1	5.1	0.32	0.05
13	305	575	11	14.3	5.6	0.30	0.04

Table 2. Average Values of C-SALT profiles

The thin high-gradient interfaces in the salt-finger thermohaline staircases are characterized by generally larger ΔT and ΔS than those observed by diffusive convection. The vertical scale of the interfaces are larger

than expected from the extrapolation of the laboratory results and this may be an important facet of the differences between observations and laboratory experiments.

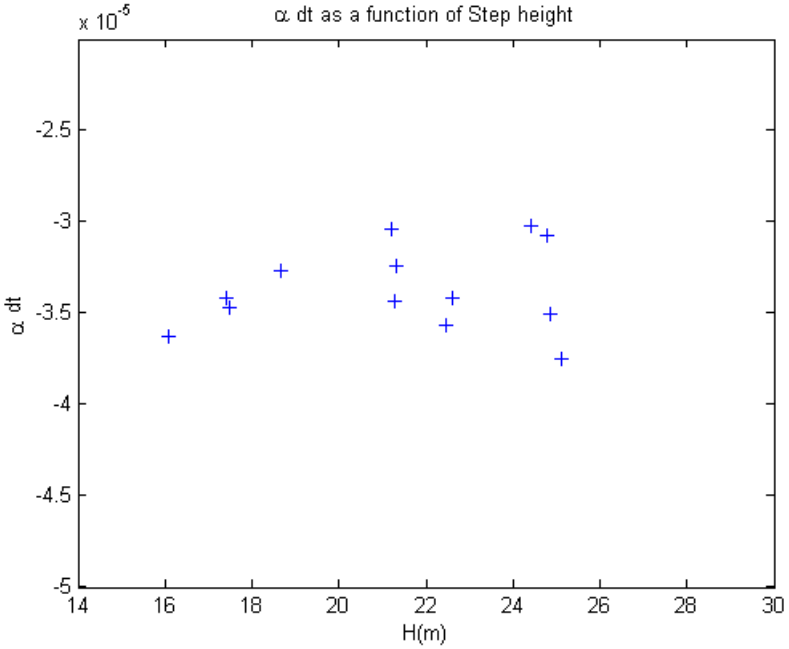

Figure 14. αΔT as a function of step height.

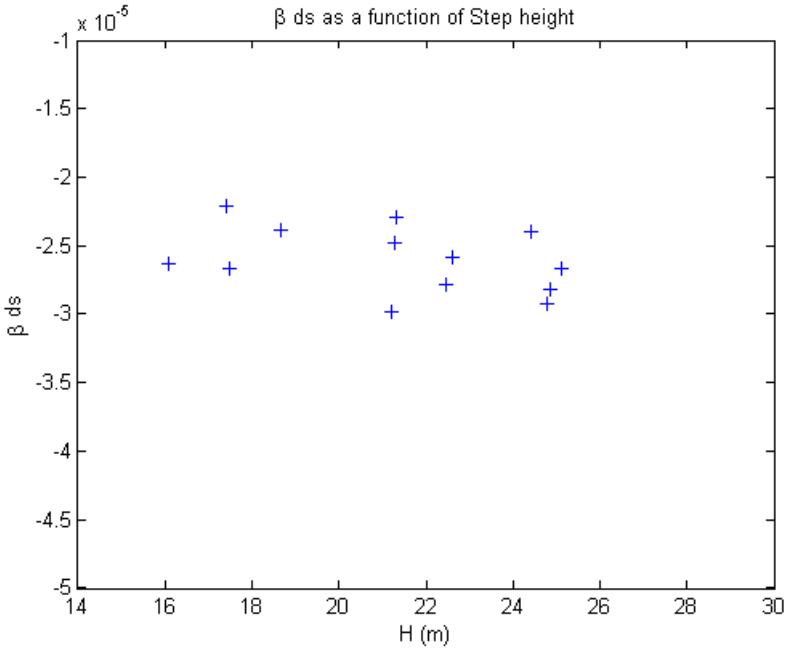

Figure 15. βΔS as a function of step height.

Figures 14 and 15 (above) show the variation of both temperature and salinity (non-dimensionalized) with step height averaged within the staircase region for each of the 13 groups identified above. As observed by Wilson (2007) for the diffusive convection case, there seems to be little dependence on the step height for either of these parameters which is consistent with Turner's (1965) assumptions used in deriving the 4/3 flux law.

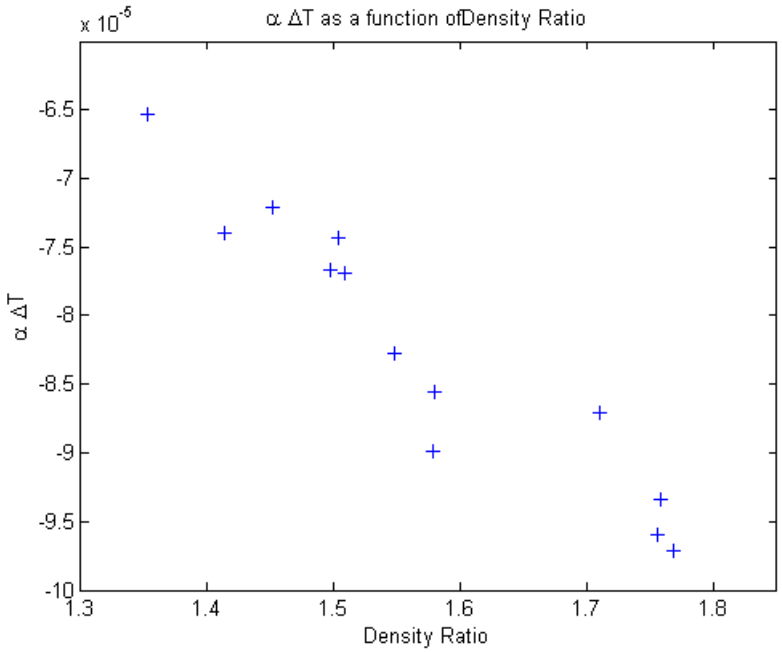

Figure 16. αΔT as a function of density ratio.

On the other both $\alpha\Delta T$ and $\beta\Delta S$ depend very strongly on density ratio, as shown in Figures 16 and 17. This indicates, albeit indirectly, that the vertical T-S fluxes in staircases also depend on R_ρ.

All these properties support the assumptions inherent in 4/3 flux law and form the basis for the calculation of the T-S fluxes.

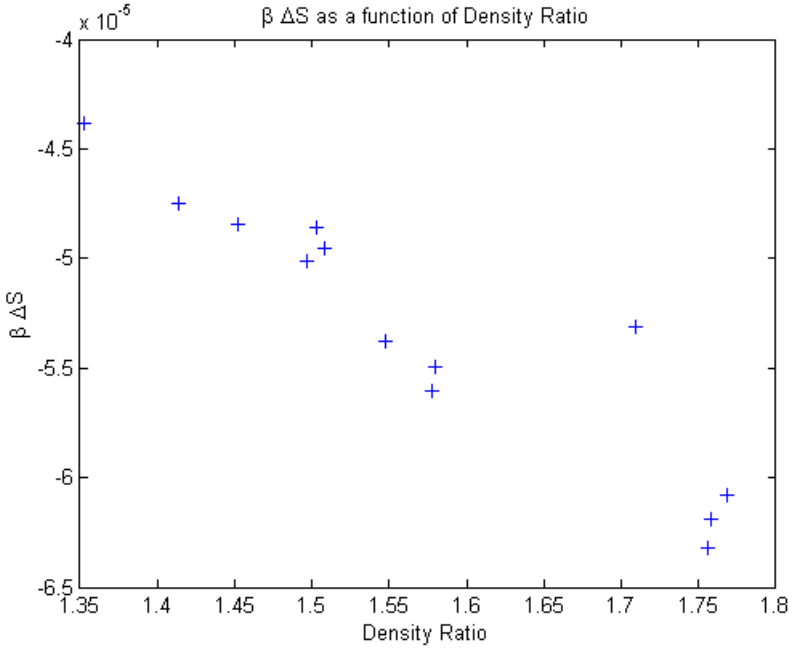

Figure 17. βΔS as a function of density ratio.

B. DENSITY RATIO OF INTERFACES

As mentioned before, the density ratio controls several key characteristics of the salt fingering process and the formation of thermohaline staircases. It is therefore essential to provide, at this point, a precise deifintion of the density ratio of thermohaline staircases. For instance as argued in Radko (2005), the density ratio across the interface can be substantially different from the density ratio based on the overall T-S variation in the step. If the steps are sufficiently thick relative to the interfaces,

does the density ratio of the layer as a whole or just the interface determine the fluxes?

The density ratio over the profile can be broken down into the density ratio over the distance between the vertical means and the density ratio of the interfaces.

Using single profiles, the density ratio of a layer and the adjoining interface for a number of stations were compared. The results are shown below.

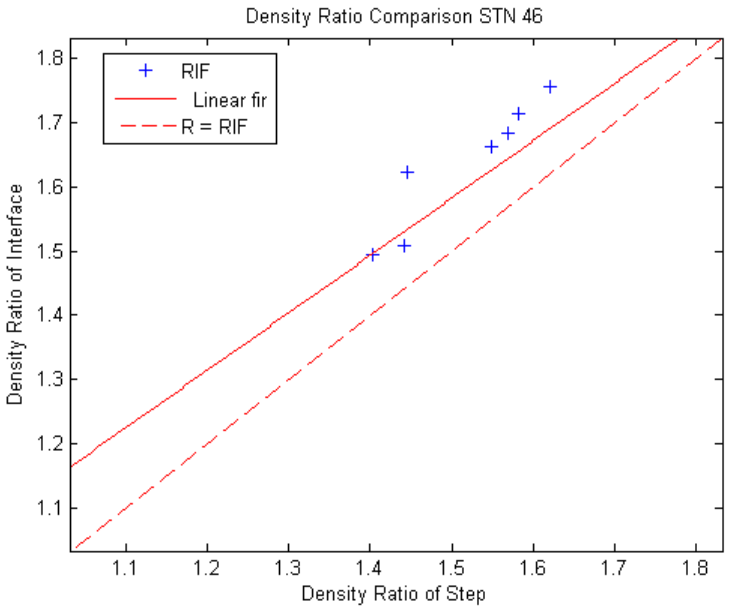

Figure 18. Density ratio comparison STN 46.

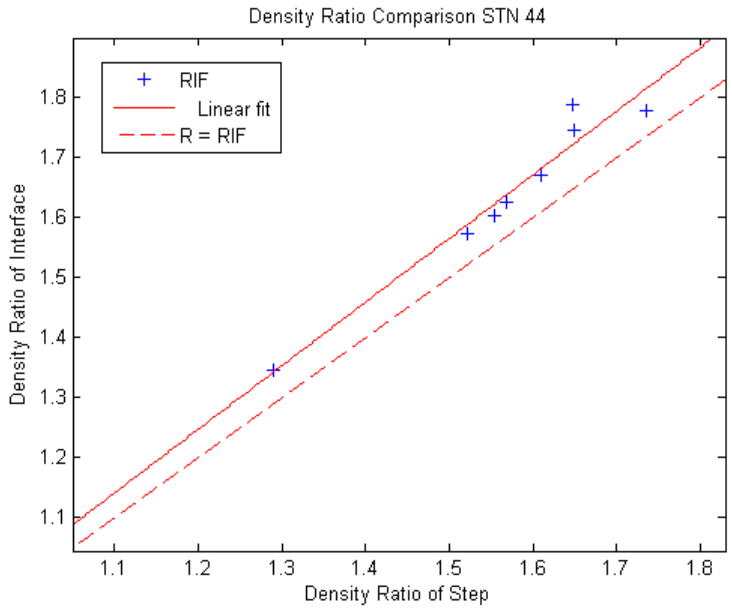

Figure 19. Density ratio comparison STN 44.

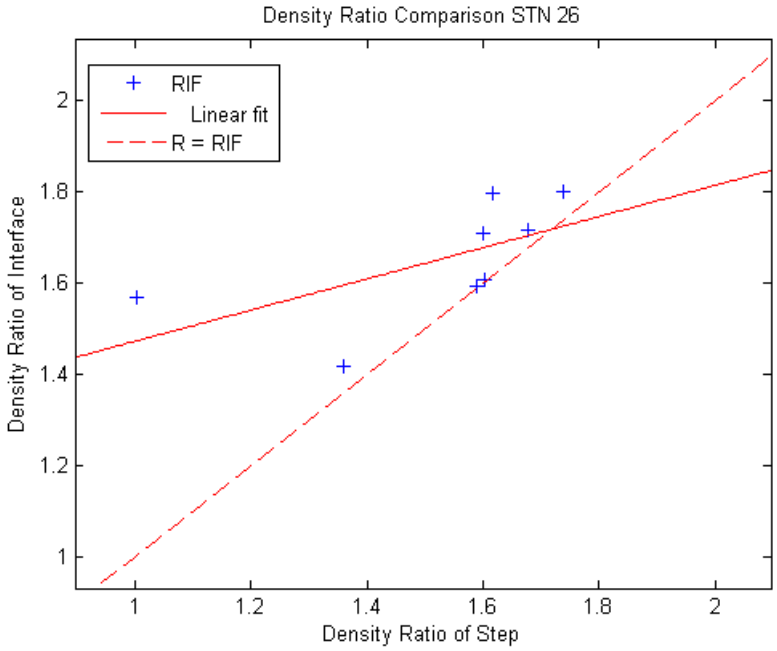

Figure 20. Density ratio comparison STN 26.

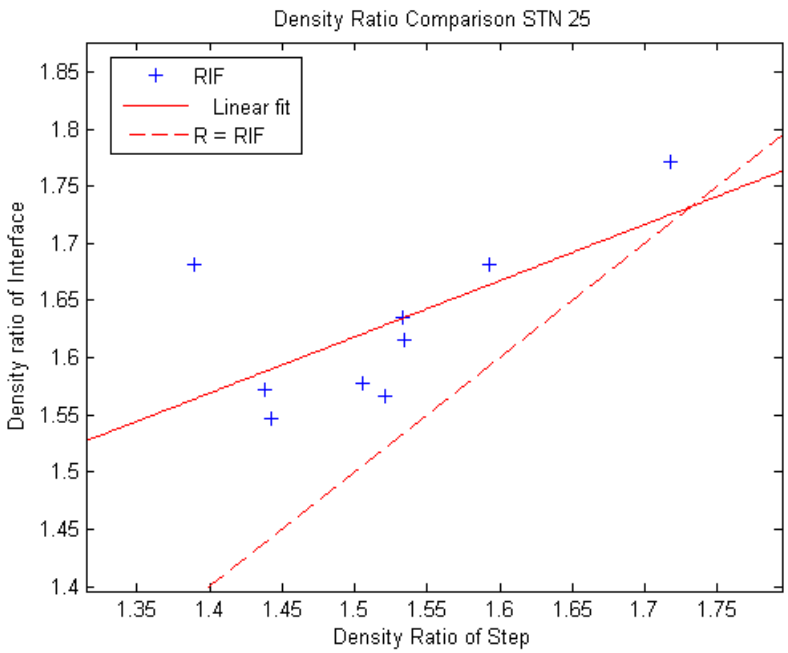

Figure 21. Density ratio comparison STN 25.

As observed by Wilson (2007) there are significant differences between the density ratios calculated over the layer and within the interface. This could be a cause of inconsistencies between observations and experimental results.

An notable observation is that the density ratio differences for the last two profiles are quite different than the first two with much greater slopes to the curves of best fit.

The last two observations are from closer to center of the staircase region observed and may be more developed and closer to the equilibrium processes suggested by Radko (2005). This may indicate that the interfaces merge until a equilibrium is reached ($R_\rho \approx 1.7$ suggested by Radko) which is close to the point where the lines of best fit cross the 1:1 ratio above.

Whilst by no means conclusive this idea is worth exploring to determine if there is significance in the differences observed in the examples above.

C. STEADY STATE THREE DIMENSIONAL ANALYSIS

Whilst many experiments and observations have explored the one dimensional structure of thermohaline staircases (in x and z), the three dimensional structure of thermohaline staircases remains poorly understood. The following analysis attempts to relate the slope of the interface to the background large-scale patterns of the temperature and salinity.

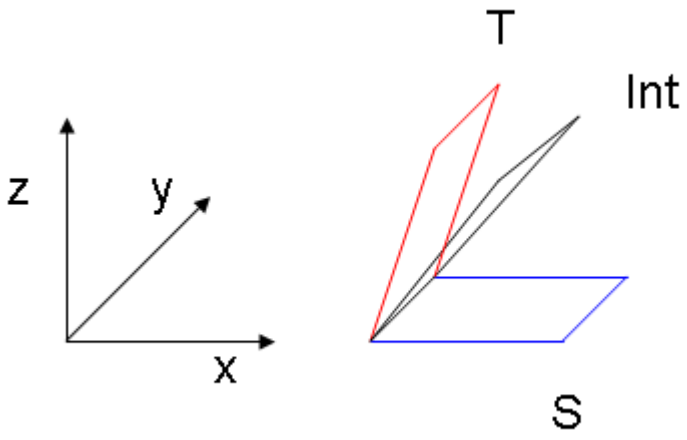

Figure 22. Configuration of two dimensional structure (where Int is the layer interface).

1. Theory

Consider the mixed layer sandwiched between two interfaces as indicated in the schematic diagram in Figure 23. The flux at the top is defined as F_2 and the bottom as F_1. Our starting point is the conservation law for temperature and salinity in the mixed layer:

$$H\frac{d}{dt}T_{12} = F_{T2} - F_{T1} \tag{6a}$$

$$H\frac{d}{dt}S_{12} = F_{S2} - F_{S1} \tag{6b}$$

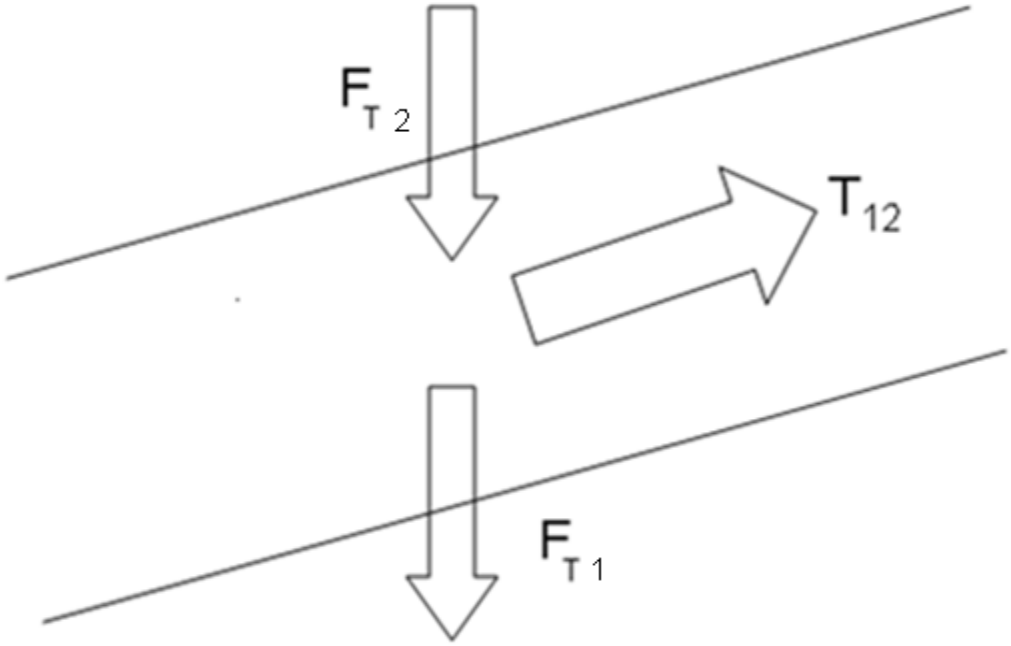

Figure 23. Basic two layer interface.

Without loss of generality, we adopt a co-ordinate system where x is in the same direction as the flow. In this case Equation (6a) can be simplified:

$$Hu\left(\frac{\partial T_{12}}{\partial x}\right)_L = F_{T2} - F_{T1} \tag{7}$$

and Equation (6b) reduces to:

$$Hu\left(\frac{\partial S_{12}}{\partial x}\right)_L = F_{S2} - F_{S1}\,. \tag{8}$$

Radko (2005) hypothesized that as staircases evolve in time to a quasi-equilibrium state, the interfacial flux ratio approaches its minimum value $\gamma_{\min}$ (Figure 7):

$$\frac{F_{T2}}{F_{S2}} = \gamma_{\min} \qquad \frac{F_{T1}}{F_{S1}} = \gamma_{\min} \tag{9}$$

Combining (7), (8) and (9), we arrive at:

$$\frac{(\partial T_{12}/\partial x)}{(\partial S_{12}/\partial x)} = \frac{(F_{T2} - F_{T1})}{(F_{S2} - F_{S1})} = \gamma_{\min} \tag{10}$$

Our next step is to reorganize that the left hand side of Equation (10) can be reduced to thwe derivative of T_{12} with respect to S_{12} along the mixed layer.

$$\left(\frac{\partial T}{\partial S}\right)_L = \frac{(\partial T/\partial x)}{(\partial S/\partial x)} \tag{11}$$

And $\left(\frac{\partial S}{\partial T}\right)_L$ can be determined from layer T-S distribution, as shown in Figure 24 (below).

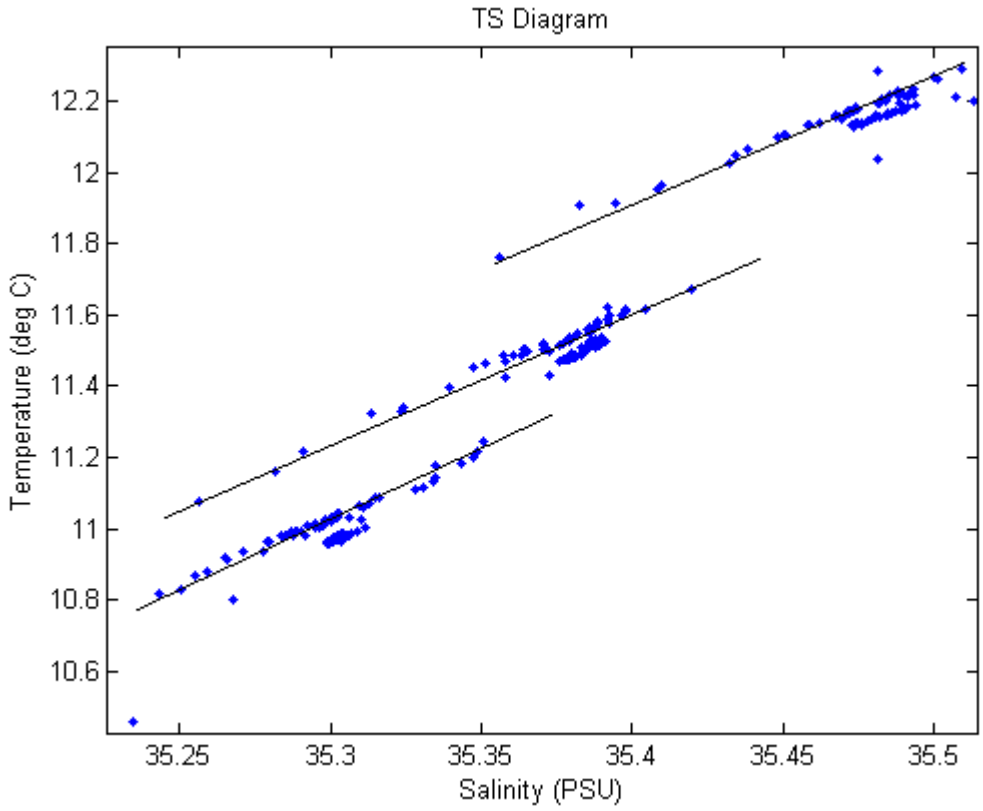

Figure 24. TS plot showing centers of layers

Attempting to develop a relationship between the slope of the layer and the background temperature gradient, we express the T-S variation along the mixed layer in terms of Cartesian derivatives:

$$\left(\frac{\partial T_{12}}{\partial x}\right)_L = \frac{\partial T}{\partial x} + tg\alpha . \frac{\partial T}{\partial z} \tag{12}$$

$$\left(\frac{\partial S_{12}}{\partial x}\right)_L = \frac{\partial S}{\partial x} + tg\alpha . \frac{\partial S}{\partial z} \tag{13}$$

where α is the slope of the interface. Dividing (12) by (13) gives:

$$\left(\frac{\partial T}{\partial x} + tg\alpha . \frac{\partial T}{\partial z}\right) = \left(\frac{\partial S}{\partial x} + tg\alpha . \frac{\partial S}{\partial z}\right)\gamma_{\min} \tag{14}$$

Equation (14) can be conveniently rewritten in terms of the background T-S gradients as follows:

$$\left(\frac{\partial T}{\partial x} / \frac{\partial T}{\partial z}\right) = -tg\alpha_T \quad \left(\frac{\partial S}{\partial x} / \frac{\partial S}{\partial z}\right) = -tg\alpha_S \tag{15}$$

where α_T (α_S) is the slope of the background temperature (salinity) in the direction of the flow.

Solving for α:

$$tg\alpha = -tg\alpha_T \frac{\partial T}{\partial z} + \gamma_{\min} * tg\alpha_S \frac{\partial S}{\partial z}) / (\gamma_{\min} \frac{\partial S}{\partial z} - \frac{\partial T}{\partial z}) \tag{16}$$

$$tg\alpha = (-tg\alpha_T * R_\rho + \gamma_{\min} * tg\alpha_S) / (\gamma_{\min} - R_\rho) \tag{17}$$

Assuming that $R_\rho > \gamma_{\min}$ then:

$$tg\alpha \approx tg\alpha_T \tag{18}$$

Thus, the key result of the foregoing model is that the interfaces should be aligned with isotherms but not necessarily with isohalines.

2. Observational Test

By this approximation, in the direction of the flow, slopes of the interfaces should be close to the slope of the isotherms and different from the slope of the salinity.

To test this theory the step feature showing the characteristics highlighted above (between 11 and 11.7^{0}C and 35.25 and 35.4 PSU) was chosen. The profiles that were well spaced and exhibited strong staircases (STNs 21 to 51) and a MATLAB code was run to extract only the vertical means that had the above characteristics.

A coordinate system was then devised based on angular deviations from the standard x, y (latitude and longitude) coordinate system. This coordinate system is defined below:

$$l_n = x\cos\varphi + y\sin\varphi \qquad (23)$$

where x is longitude and y is latitude and φ is the angle of interest . Figure 25 (below) shows value of φ ranging from 30^0 (orange) to 180^0 (black).

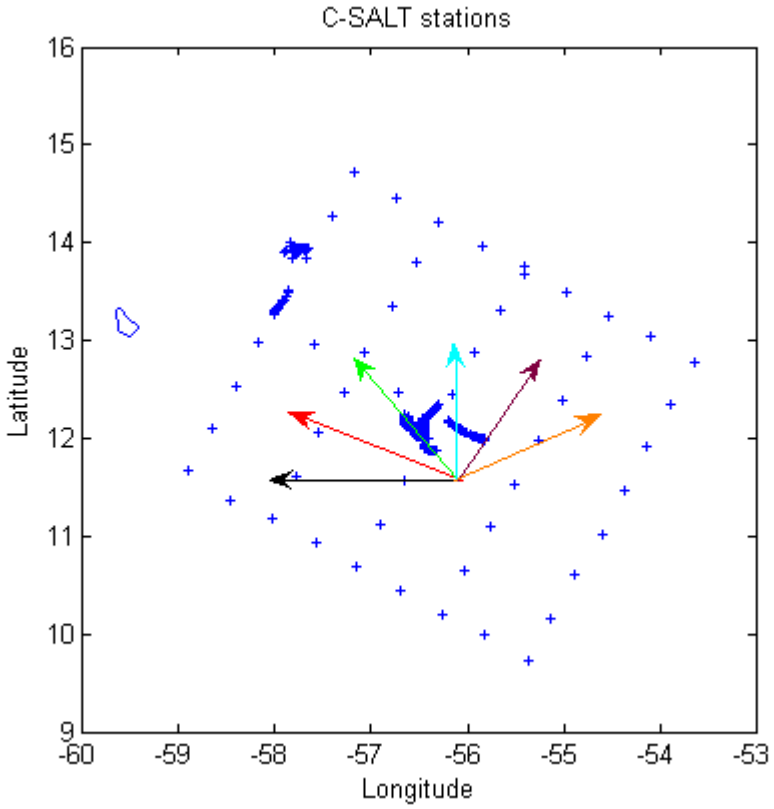

Figure 25. Definition of angle φ

Using this coordinate system, the positions of the STNs identified were calculated and the dependence of T and S on l_n in the new coordinate system was determined. The foregoing analysis suggest that the slope of the interface should be close to that of the large-scale isotherms as long as φ is close to the mean background flow in the area.

To estimate the direction of the mean flow, we used a numerical model (Radko et. al. 2007) which is based on the GFDL MOM3 code (Pacanowski and Griffies 1999). The horizontal resolution is 2° in longitude and latitude. The model domain is global and extends from 78°S to 84°N. There are 25 levels in the vertical with resolution increasing from 17m at the surface layer to 510m at the bottom.

The direction of the mean flow indicated by the model is largely westward (ranging from 265 at 220m to 274 at 370m) which corresponds to a φ value of 180 in the new coordinate system.

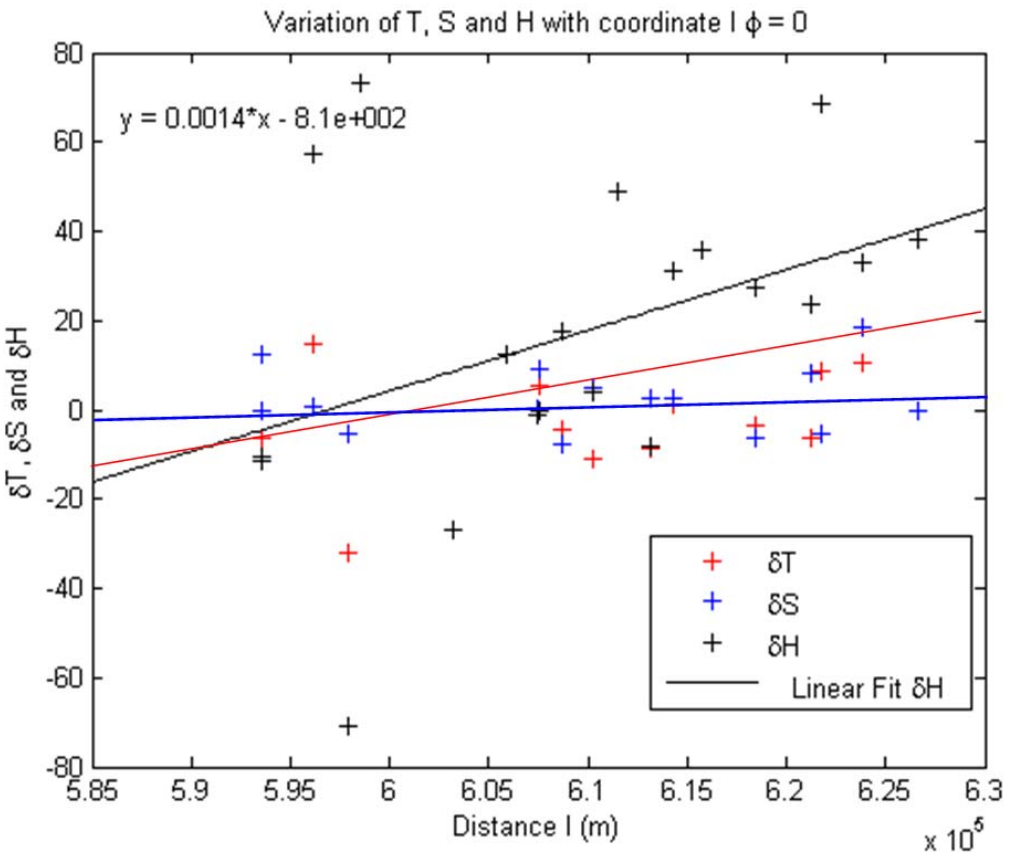

Figure 26. ΔT, S and H as a function of l when φ = 0 (equivalent to 180)

As shown above the relationship between the isotherms and the slope of the layers is stronger than that of the isohalines.

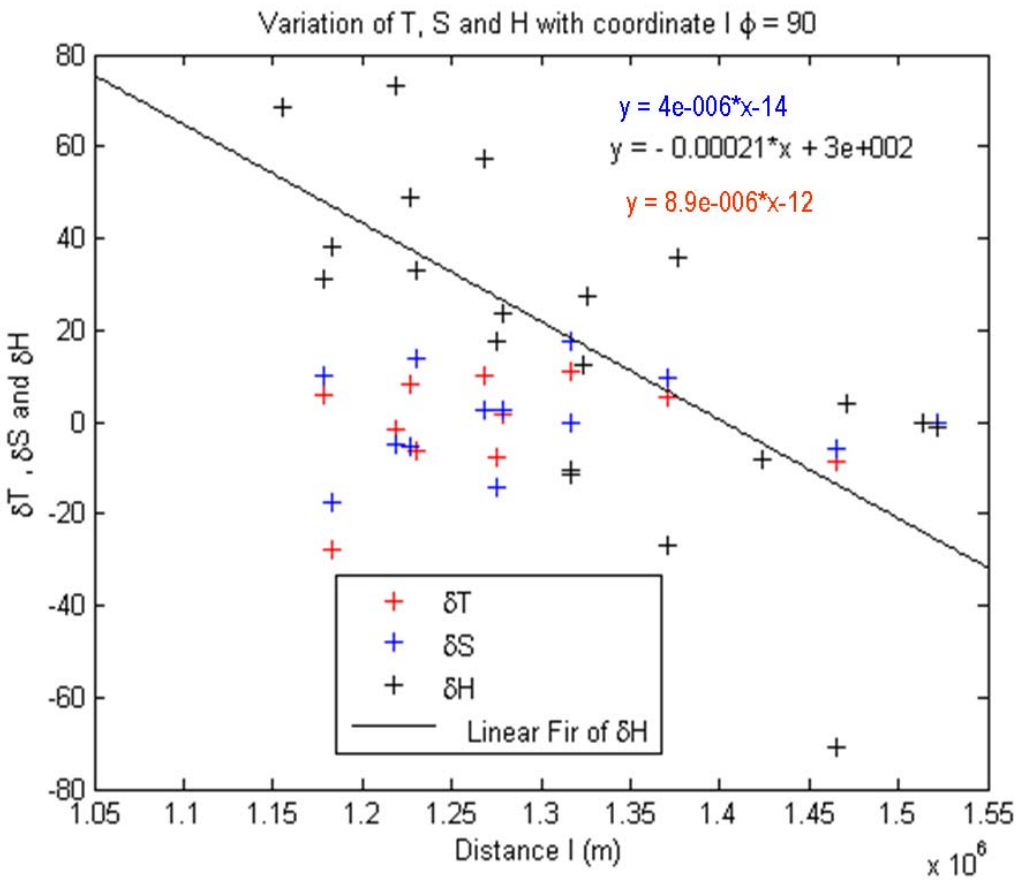

Figure 27. ΔT,S and H as a function of l when φ = 90

As φ is moved further from the direction of flow, the relationship between the isotherms and the slope of the interface becomes very different from that predicted by our theoretical model [Equation (18)].

An example of the calculation for φ which is not oriented in the direction of the background flow is shown in Figure 27.

This preliminary investigation is promising and is worth further exploration to explore the relationship between the isotherms and the slope of the layers.

THIS PAGE INTENTIONALLY LEFT BLANK

III. EVOLUTIONARY PATTERNS OF THERMOHALINE STAIRCASES

A. BACKGROUND

In order to determine whether thermohaline staircases are significant from an ocean mixing perspective it is imperative to determine the associated fluxes of heat and salt. These fluxes can then be parameterized for ocean models and can assist in determining the role that double diffusion has in the transport of heat and salt in the thermocline.

A number of earlier attempts to quantify the T-S fluxes in the staircases include the tracer release experiment (Schmitt et. al. 2005) aimed at measuring the fluxes in the western tropical North Atlantic.

We offer an alternative approach, in which fluxes are related to the rate of merging events identified in moored profiler data. Another key outcome of this calculation is the indirect validation of the merging theory for the ocean.

1. Previous Studies

A theory for merging events was introduced by Radko (2003) proposing that the formation of layers in a double-diffusive liquid starts in the form of growing, horizontally uniform perturbations that transform the gradient into a stepped structure consisting of salt finger interfaces sandwiched between nearly homogenous layers. Layers that develop merge continuously (strong layers at the expense of weaker layers) increasing the step height (the nearly homogenous layer) until equilibrium is reached ($H > H_0$, Radko

2005). This theory directly connects the vertical T-S fluxes to the rate of merging events (Radko 2007, Wilson 2007).

Pursuing this idea further, we now attempt to estimate fluxes by examining a number of merging events identified in moored profiler data provided by John Toole from Woods Hole Oceanographic Institute.

B. MERGING EVENTS

1. Data Source

A moored profiler was located at 13^0N 55^0W and recorded 775 profiles of the temperature, conductivity (salinity), pressure and velocity of the water column between 100 and 700m over 129 days between February and July 2001. The location of the moored profiler and information on data from the SFTRE is shown in Chapter II.

For more information on the moored profiler the readers are referred to the website Moored profiler homepage (Nov, 2007).and Doherty, et. al. (1999)

2. Merging Theorem

In order to apply the merging theorem (Wilson 2007) to actual field data, explicit expressions for fluxes are needed. While little is known about the flux laws in the ocean, we assume that the general structure of the laboratory-derived flux laws pertain to the ocean, but additional calibration of amplitude is necessary. Adopting the derived 4/3 flux laws, but recalibrating them for oceanic conditions, yields:

$$\left.\begin{aligned} \alpha\tilde{F}^T &= AC(\alpha\Delta T)^{4/3}; \quad C = F(R_\rho) \\ \beta\tilde{F}^S &= \alpha\tilde{F}^T\gamma; \quad \gamma = F(R_\rho) \end{aligned}\right\} \tag{19}$$

Where "A" is an adjustable coefficient included to recalibrate flux laws for the ocean. The coefficient C and γ are both a function of density ratio (the form of the function is discussed later). The solution to the growth rate as shown by Wilson (2007), is:

$$\lambda_B = \frac{4}{H}\frac{\frac{\partial\tilde{F}^S}{\partial\tilde{T}}\frac{\partial\tilde{F}^T}{\partial\tilde{S}} - \frac{\partial\tilde{F}^T}{\partial\tilde{T}}\frac{\partial\tilde{F}^S}{\partial\tilde{S}}}{\frac{\partial\tilde{F}^T}{\partial\tilde{T}} + \frac{\partial\tilde{F}^S}{\partial\tilde{S}}} \tag{20}$$

Simplifying this equation using Equation (19):

$$\lambda_B = \frac{(\alpha\Delta T)^{\frac{1}{3}}}{H}F(R_\rho) \tag{21}$$

Where $F(R_\rho)$ depends on the particular forms of C(R_ρ) and $\gamma(R_\rho)$.

Now, we apply the foregoing model to moored data. The exponential variation of $\Delta T, \Delta S$ across the merging layers confirms the interpretation of the merging as an instability process. The growth rate of each merger is determined from the best fit of the exponent $\exp(\lambda t)$ to $(\Delta T - \Delta T_0)$, where ΔT, is the temperature variation in the merging layer, and ΔT_0 is its value at the beginning of the merging event.

There were four merging events identified from the moored profiler data and they are shown in Figures 28 and 29 (below).

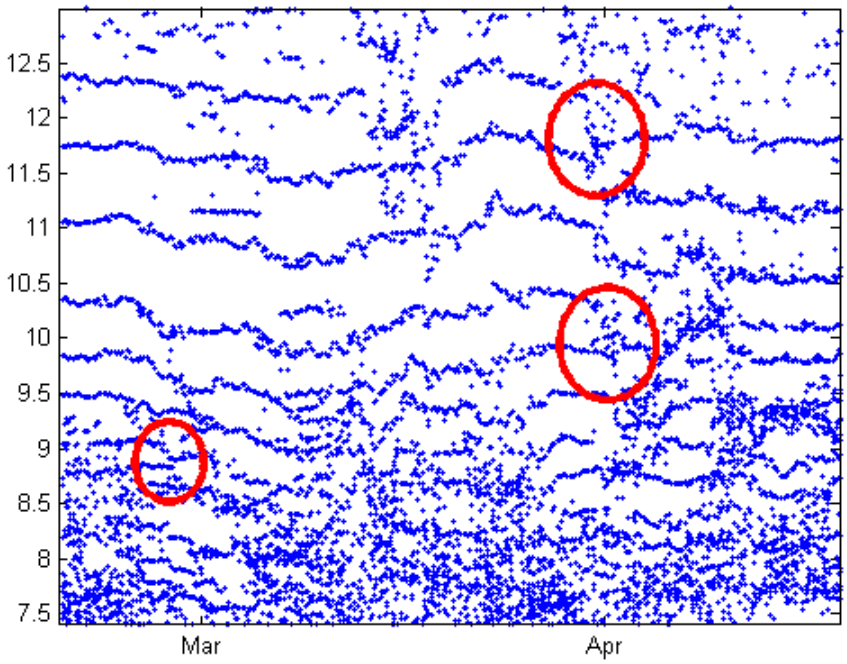

Figure 28. Merging Events 1 to 3 (1 top, 3 bottom)

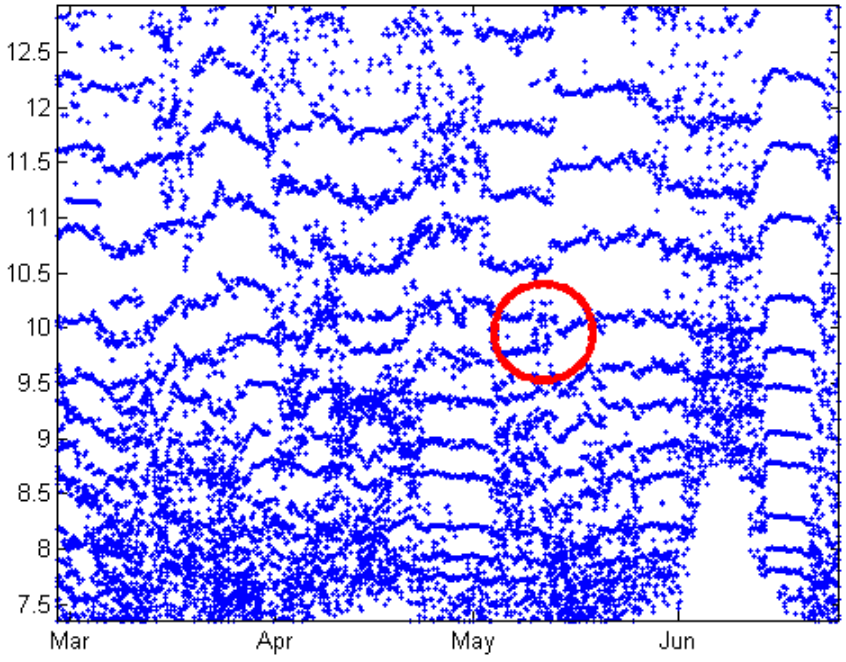

Figure 29. Merging Event 4

3. Flux Calculations

Figures 30 and 31 (below) show the change in temperature as a function of time for two of the merging events.

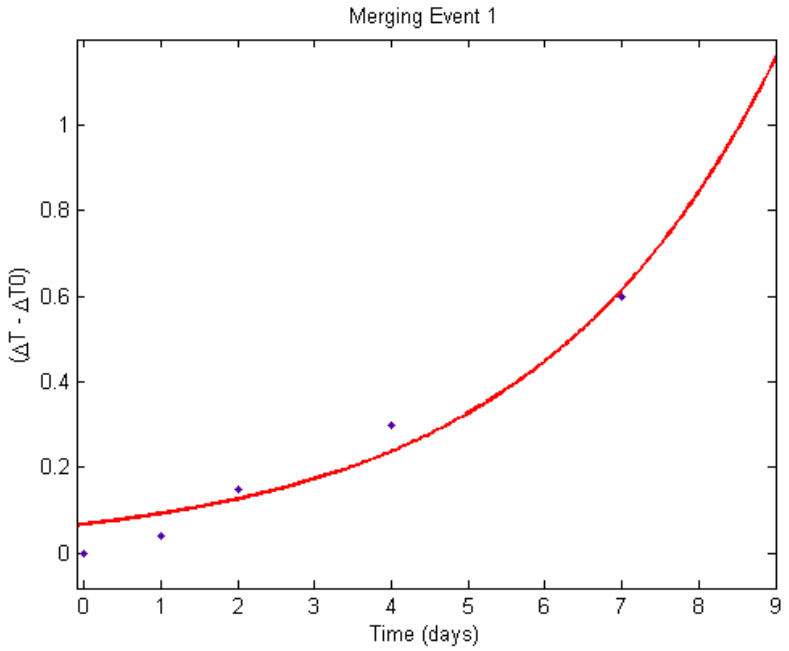

Figure 30. Change in temperature vs. time during Merging Event 1

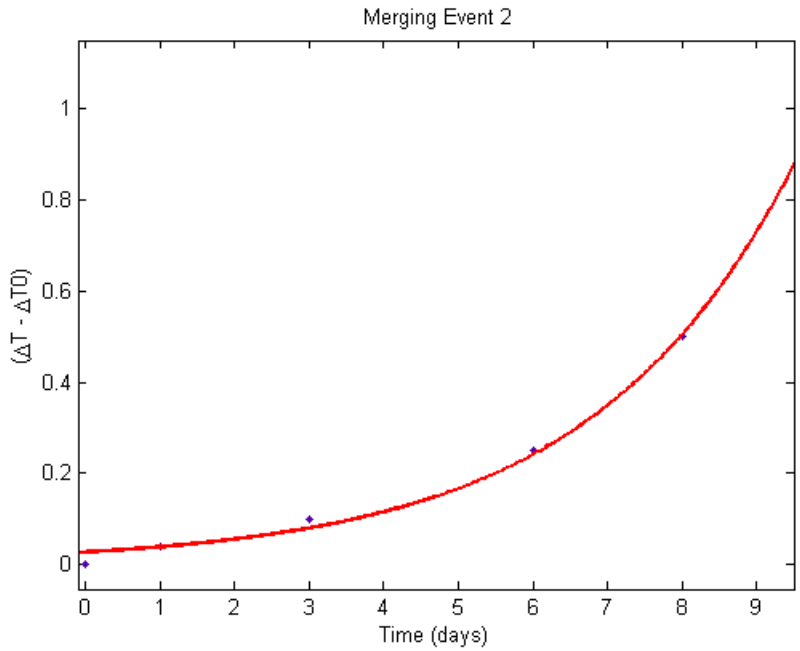

Figure 31. Change in temperature vs time during Merging Event 2

The merging periods vary from 6 to 10 days and 0.45 to 0.85 deg C.

The merging growth rates are normalized as follows:

$$\lambda_{NORM} = \frac{\lambda_B H}{(\alpha \Delta T)^{\frac{1}{3}}} \tag{22}$$

and the data from the Merging Events is tabulated below:

Merging Event	Growth Rate (10^{-6})	ΔT (deg C)	ΔS (PSU)	H (m)	Density Ratio	Normalized Growth Rate (10^{-4})
1	2.66	0.65	0.1	15	1.62	7.88
2	2.82	0.6	0.11	20	1.36	11.43
3	3.68	0.65	0.1	15	1.47	10.09
4	2.88	0.55	0.08	10	1.72	6.01

Table 3. Data from Merging Events 1 to 4.

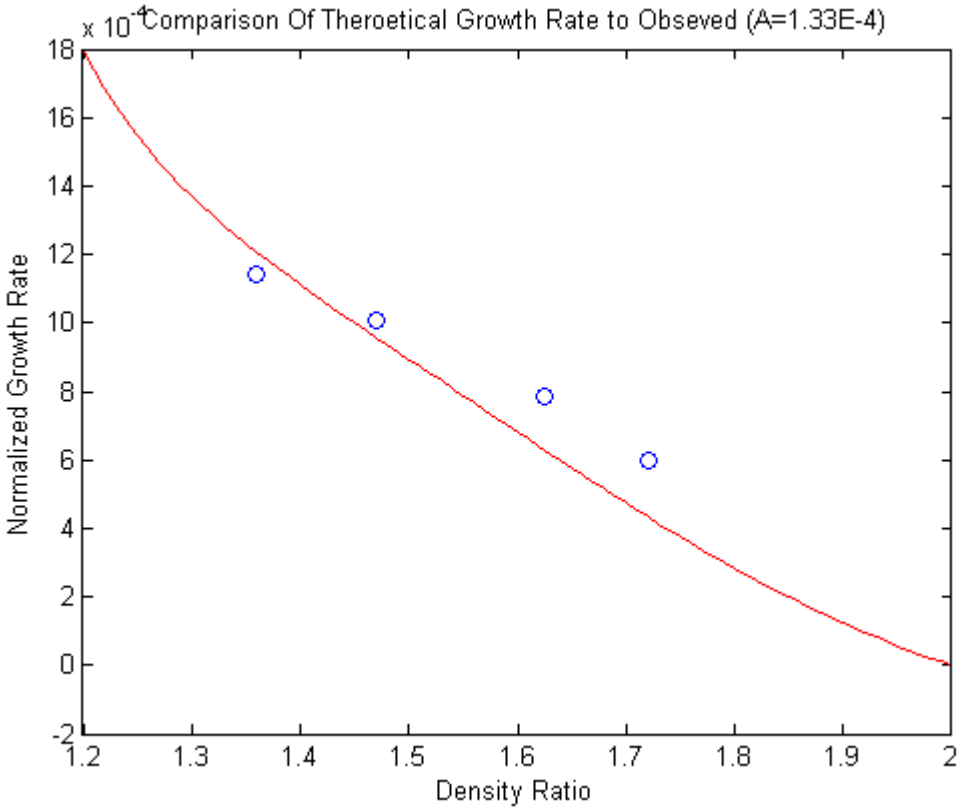

Figure 32. Plot of the calculated normalized growth rate versus density ratio for the Merging Events compared to the Theoretical Value.

To calculate the fluxes from the data we ; i)introduce the specific structure functions for the flux law coefficient and ii) assume a simple explicit form for the flux ratio, γ , both of which are consistent with laboratory experiments.

Radko (2005) discussed the relationship between flux ratio and density ratio and formulated an expression that closely follows the laboratory results closely for the interval we are interested in $(1.1 < R_\rho < 2.)$.

$$\gamma = 0.6 + \frac{(R_\rho - 2)^2}{2.5} \tag{23}$$

The curve is compared with theoretical results in Figure 33.

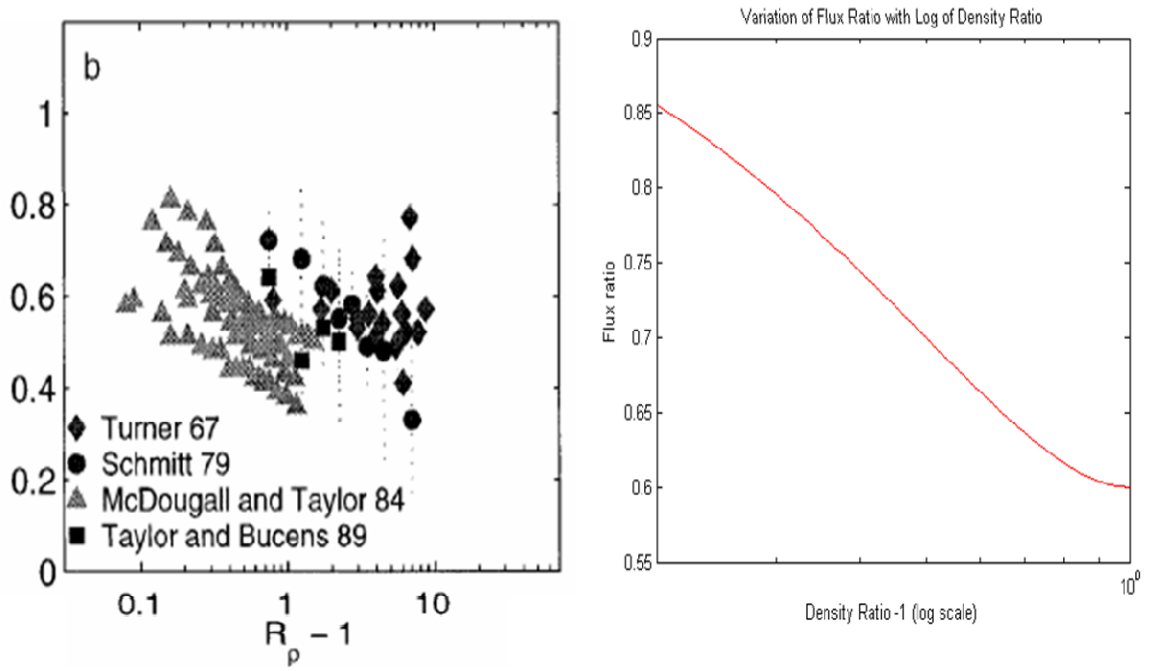

Figure 33. Flux ratio comparison (Left from St Laurent 1999).

To determine the coefficient C in the flux law, calculations were made attempting to mimic the change in C with density ratio fit to laboratory measurements (Kunze 2003). We adopt the structure function $C = \frac{1}{\sqrt{R_\rho - 1}}$ which is plotted below.

Note that a factor of 0.1 was applied to the structure function to make it easier to visually compare 'C' with the pattern of laboratory distribution. (right panel of Figure 34).

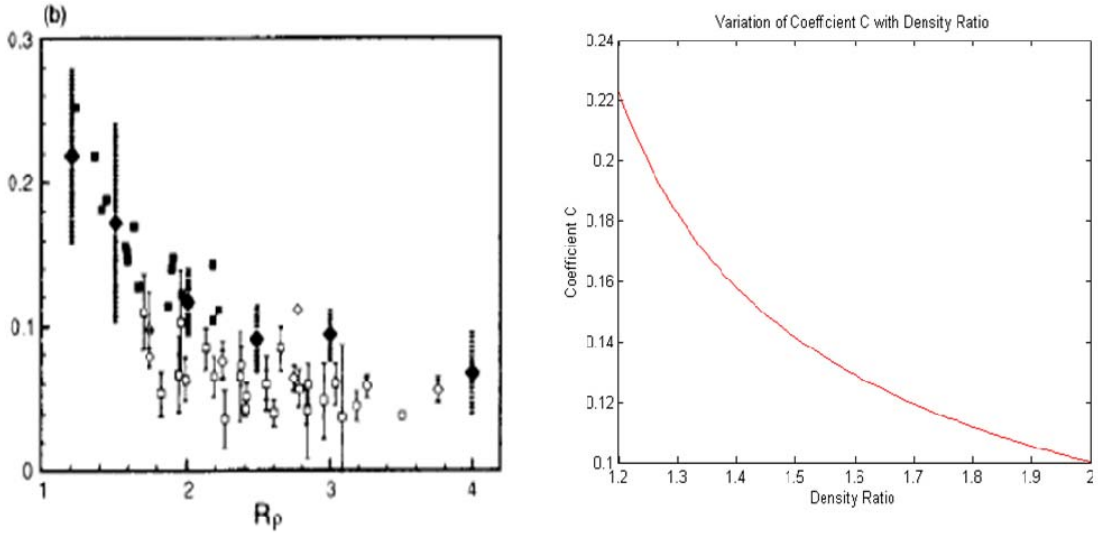

Figure 34. Coefficient comparisons (Left from Kunze 2003)

The value of A is then determined by calculating the least difference between the theoretical normalized growth curve and the normalized growth rates, resulting in A = 1.33 x 10^{-4}m/s.

Merging Event	Growth Rate (10^{-6})	ΔT (deg C)	Coefficient A (10^{-5})	H (m)	Density Ratio	Temperature Flux (10^{-10})
1	2.66	0.65	9.0	15	1.62	7.49
2	2.82	0.6	9.4	20	1.36	9.27
3	3.68	0.65	9.25	15	1.47	8.85
4	2.88	0.55	9.5	10	1.72	5.94

Table 4. Flux calculations from Merging Events 1 to 4.

Using 1.33 x 10^{-4} m/s for A and $C = \frac{1}{\sqrt{R_\rho - 1}}$, a theoretical curve for temperature flux as a function of density ratio was calculated using Equation (26).

The dependence of the flux on density ratio predicted in Equation (19) is shown in Figure 35. The range fo fluxes estimated from tracer release experiments by Schmitt (2005) is indicated by the filled rectangle. The latter were estimated using:

$$\alpha F_T = \alpha \kappa_T \frac{\partial T}{\partial z} \qquad (24)$$

where κ_T is the overall eddy diffusivity. The tracer release experiment (Schmitt et. al. 2005) suggest the value of κ_T = 0.45 x 10^{-4} m/s. The range of $\frac{\partial T}{\partial z}$ was inferred from the C-SALT profiles. The horizontal extent represents the range of the density ratio for the same profiles.

The theoretical dependence (Figure 36) for the salinity flux is determined using Equation (19). And the estimates

based on the tracer release experiment is indicated by the filled rectangle. The latter uses:

$$\beta F_T = \beta \kappa_S \frac{\partial S}{\partial z} \tag{25}$$

where κ_S is the vertical eddy diffusivity of salt. The value of κ_S (0.9×10^{-4} m/s) was also determined by Schmitt (2005) and the vertical extent of the rectangle indicates the range of $\frac{\partial S}{\partial z}$ values calculated from the C-SALT profiles.

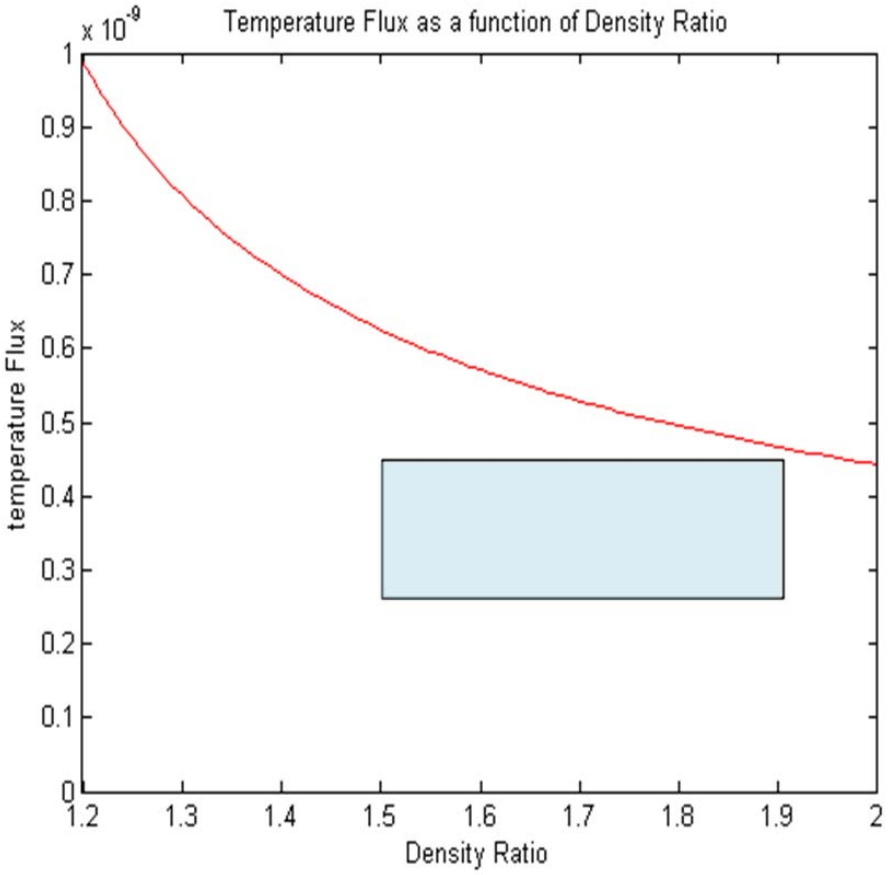

Figure 35. Temperature flux as a function of Density Ratio

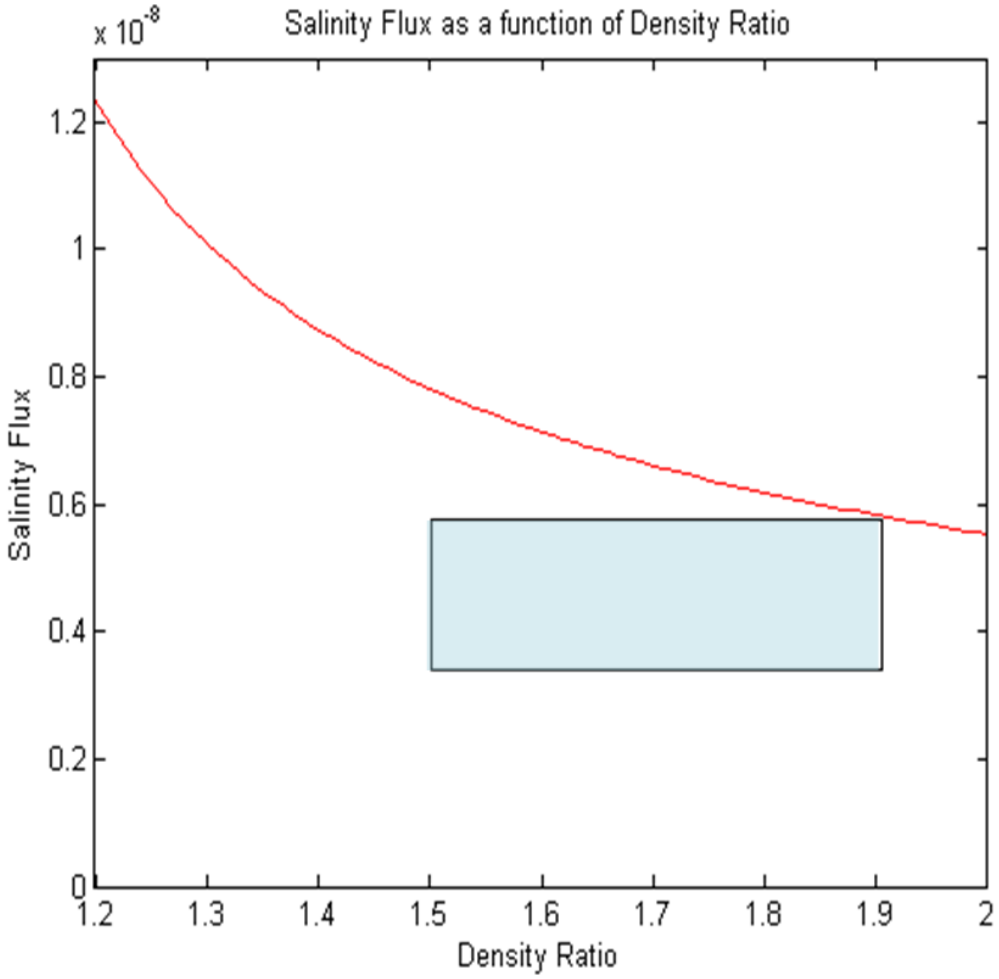

Figure 36. Salinity flux as a function of Density Ratio

With regard to the values of fluxes in Figures 35 and 36, we note that historically, models of the meridional overturning were focused on effects of the thermodynamic forcing of the individual density components (Stommel 1961), and the vertical mixing was invoked as a means for communicating the buoyancy signal between the surface and the ocean interior (Munk, 1966). However, several recent findings, theoretical and observational, cast some doubt on

the ability of purely diffusive models to explain the magnitude and pattern of the meridional overturning. While numerical simulations of the Atlantic indeed exhibit a dependence of the Meridional Overturning Circulation (MOC) on diapycnal diffusivity (e.g. Bryan 1987), most diffusive models have to rely on very high values of vertical mixing ($5\text{-}10\times10^{-5}$ m^2s^{-1}) to reproduce overturning of realistic strength. Such high values are not supported by the microstructure and tracer dispersion measurements in thermocline regions devoid of the pronounced staircases where the thermocline diffusivity of the order of 1×10^{-5} m^2s^{-1} (Ledwell et al. 1993; Toole et al 1994). The staircase regions therefore may allow maintenance of the MOC and the great conveyor belt circulation through the fundamentally diffusive mechanisms.

THIS PAGE INTENTIONALLY LEFT BLANK

IV. ACOUSTIC PROPAGATION THROUGH THERMOHALINE STAIRCASES

A. BACKGROUND

1. Previous Studies

Chin-Bing et al (1994) have studied the effects of thermohaline staircases on acoustic propagation off the South American coast in an area neighboring the C-SALT experiment. In this study a high resolution stepped profile was compared to a standard depth profile and historical data. A frequency of 50Hz was used, which coincided with an acoustic wavelength of the same order as the size of the steps. A notable conclusion from this study was that both source and receiver were required to be within the staircases for significant differences between acoustic predictions with and without the ``steps'' (up to 10dB) to be observed.

Wilson (2007) also investigated the effects of thermohaline staircases but focused on structures caused by diffusive convection in the Beaufort Gyre. Using the Bellhop model (Gaussian ray projection) for a 3500Hz source, the results indicated that significant differences in acoustic predictions (up to ±15dB) could be observed between smoothed and stepped profiles. Importantly, at this higher frequency, Wilson's results indicated that the receiver need not be within the staircases to have an effect on the acoustic propagation.

In this thesis we build upon the previously described work by examining acoustic propagation at several frequencies, and source depths utilizing staircases observed during the C-SALT experiment

B. PROCESS

1. Profile

A profile was selected from the C-SALT profiles (STN 46) that had staircases evident from approximately 230m to 530m.

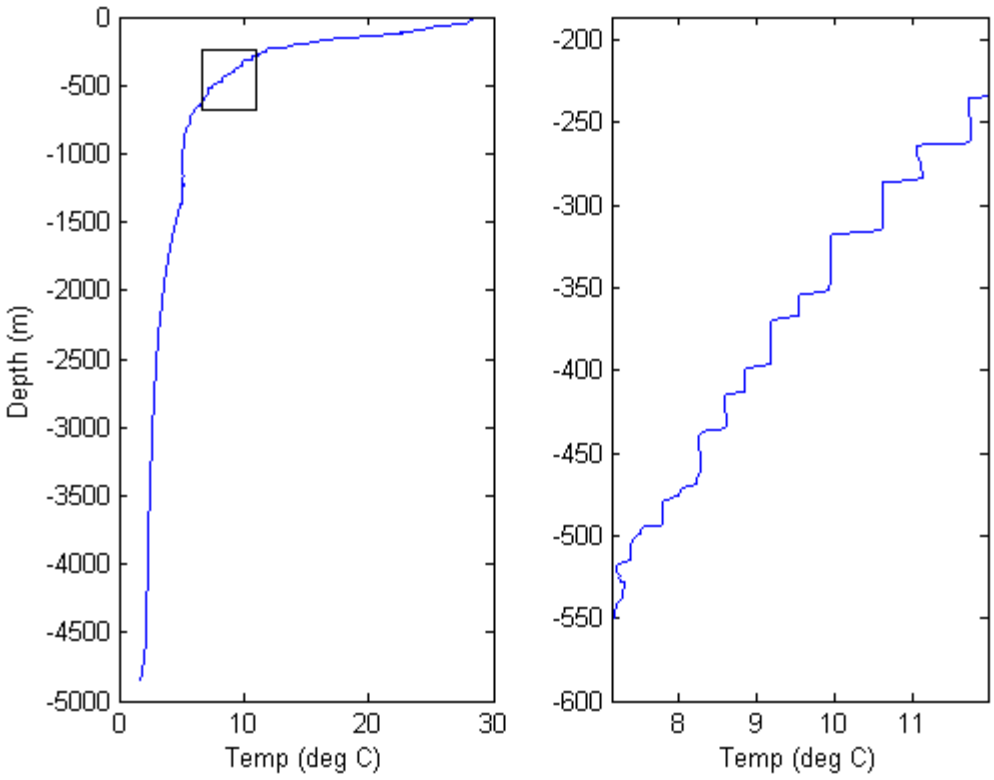

Figure 37. Temperature Profile STN46 (left hand side is zoomed in.)

The sound speed profile was then calculated using the sw_svel function of the Sea Water toolbox in MATLAB. The sound speed profile is shown below. The saw tooth pattern is a common feature of the staircases as the steps are almost isothermal and the increasing pressure leads to an increase in sound speed for each step.

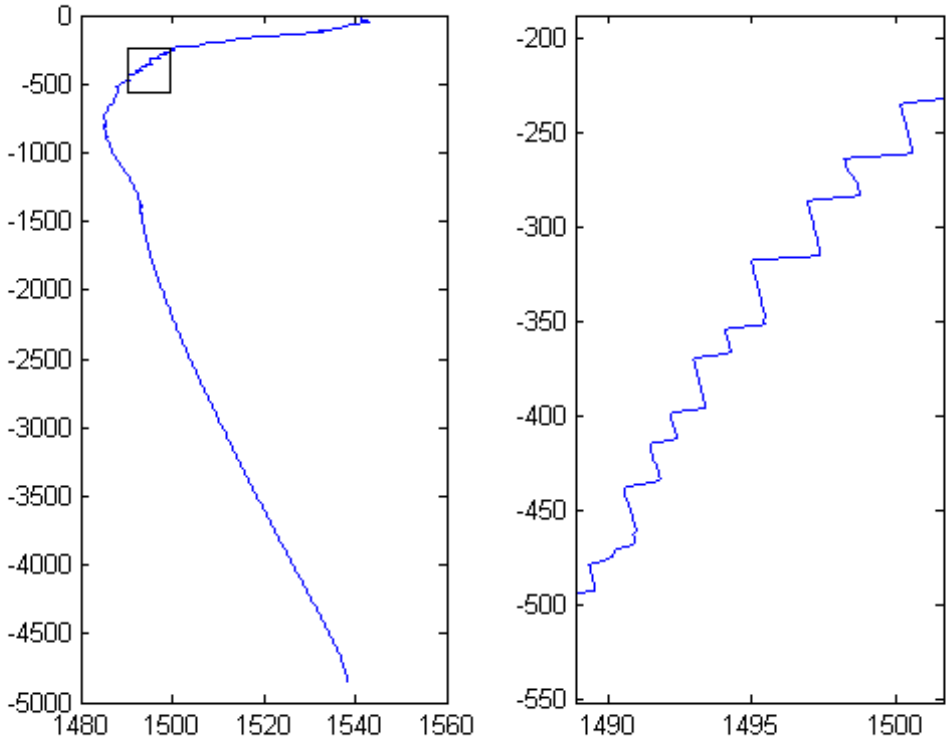

Figure 38. Sound speed profile STN46.

The profile was smoothed using a digital filter (4-pole Butterworth) to remove all influences of the sharp changes in sound speed (including the thermohaline staircases evident from 230 to 530m.) The smoothed profile is shown below.

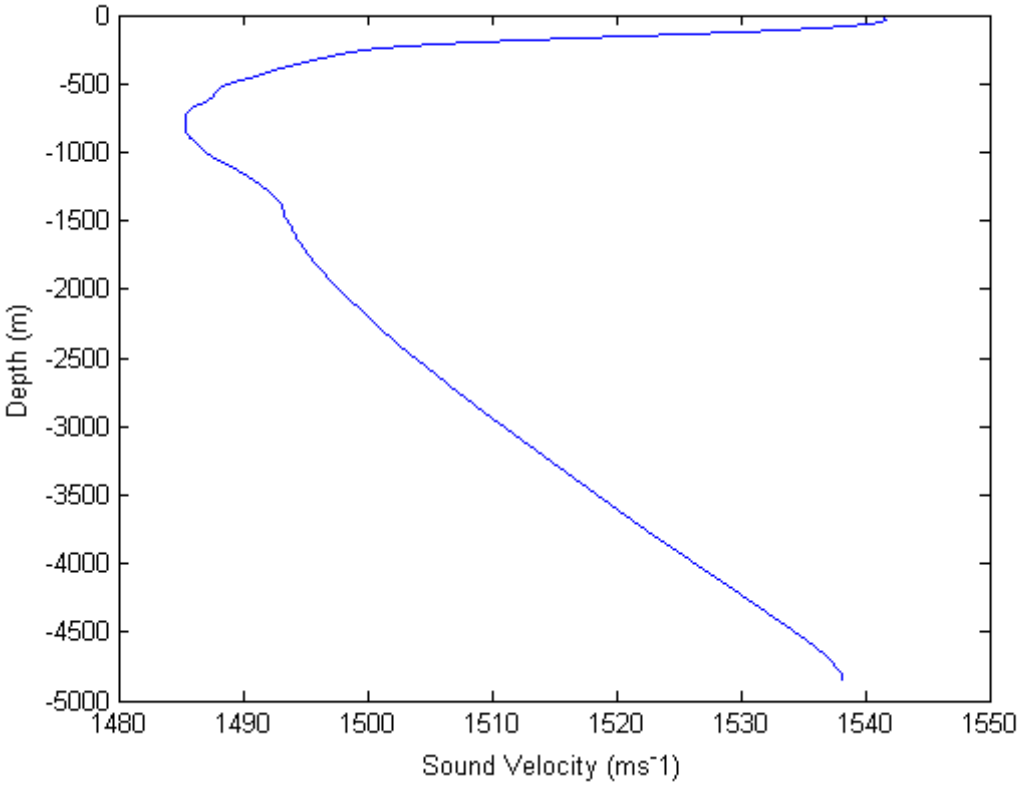

Figure 39. Smoothed profile.

The stepped region was extracted from the original profile and appended to the smoothed profile with the result shown below. Note the reduced gradient part of the profile around 1400m is evident in both profiles.

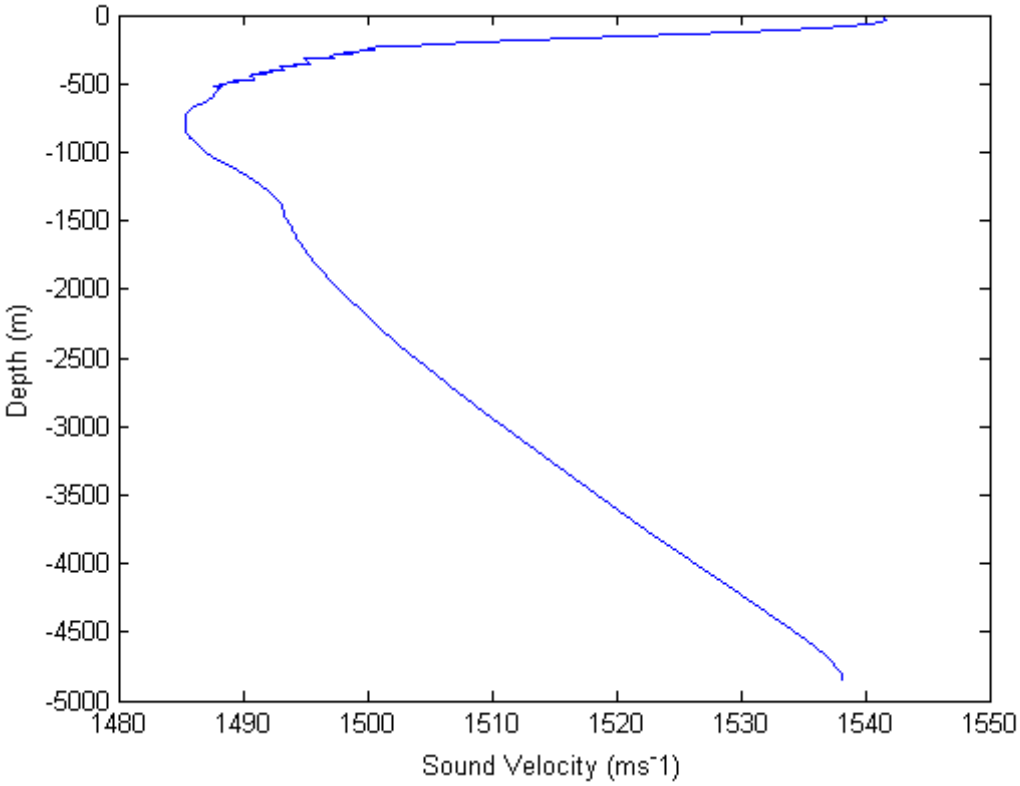

Figure 40. Stepped profile.

The differences between the profiles are highlighted in the next figure which is zoomed in to show that the only difference in the profiles is due to the presence of the thermohaline steps.

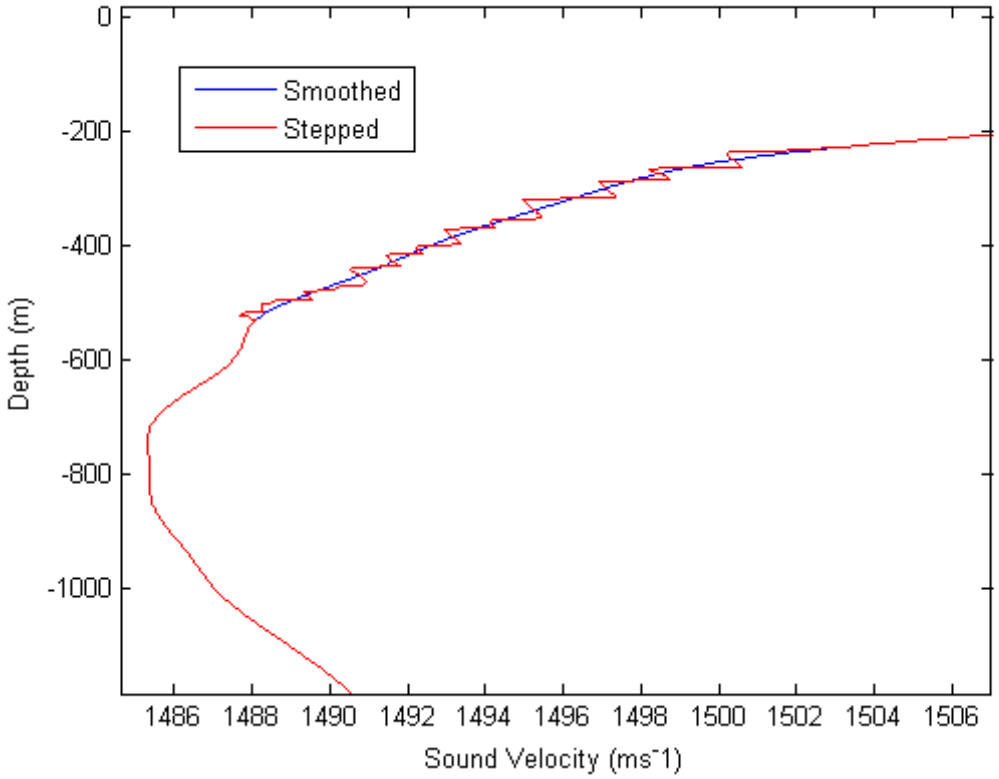

Figure 41. Profile differences highlighted.

2. Parabolic Equation Model

In order to determine what effects the steps may have on acoustic propagation, a Parabolic Equation (PE) model was run for both profiles, smoothed and stepped.

The PE model was then run for different source depths (400 and 800m) and different frequencies (50Hz, 400Hz and 1200Hz) to observe if the effects of the staircases. An important issue is the relative effects of the staircases when the source is located inside/outside of the staircases, and if the result is sensitive to acoustic frequency.

The parameters for horizontal and vertical resolution were set at 5m and 1m respectively.

C. RESULTS

The first model runs were using 400Hz and a source depth of 400m (within the staircase region). It was proposed that if the source was within the staircase region that there would be greater differences between the predictions with and without the steps (as observed by Chin-Bing et al.)

1. Source Depth 400m

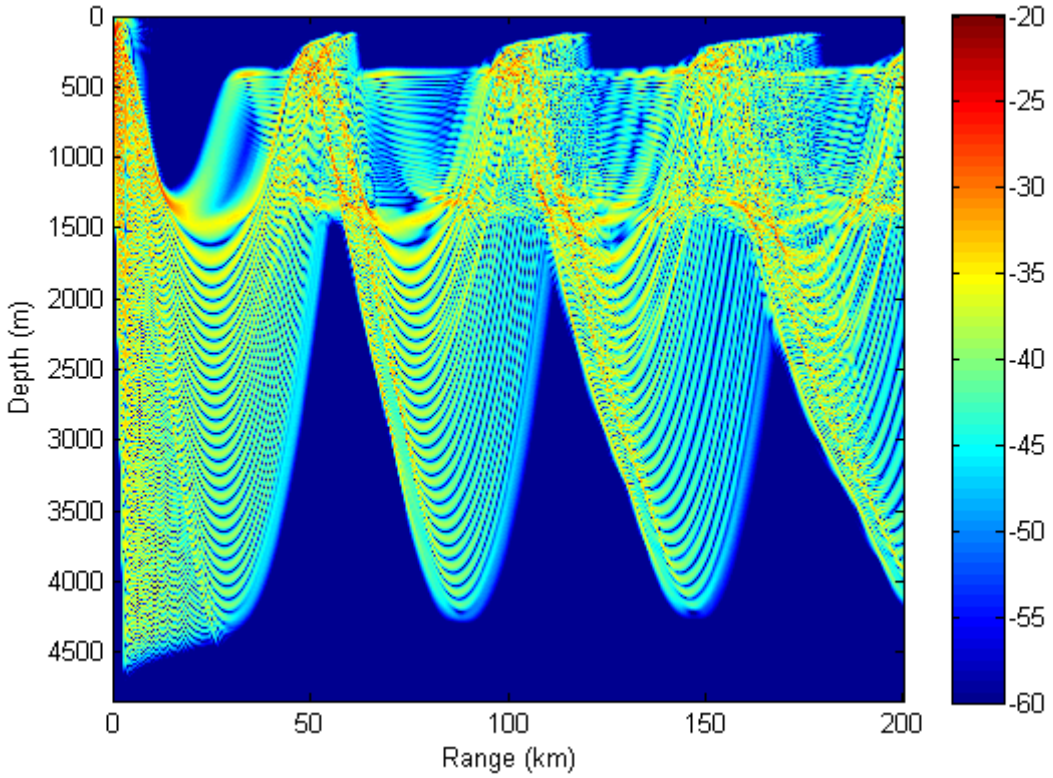

Figure 42. Smoothed Source Depth 400m.

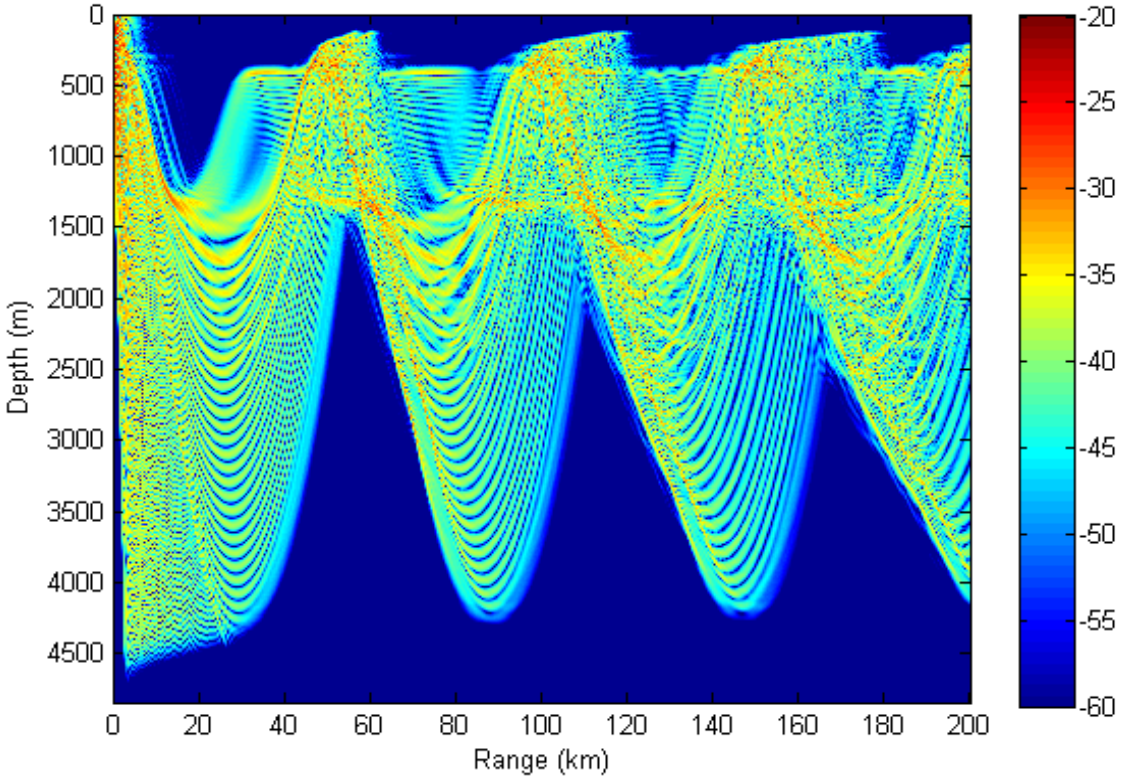

Figure 43. Stepped Source Depth 400m.

Qualitatively, the smooth profile result is more regular than the stepped profile result and the reduced gradient area in 1400m causes a secondary channel that turns at around 400m as opposed to around 150m for the majority of the acoustic energy.

The stepped result was compared with the smoothed profile to highlight the differences on the acoustic propagation evident due to the presence of the steps.

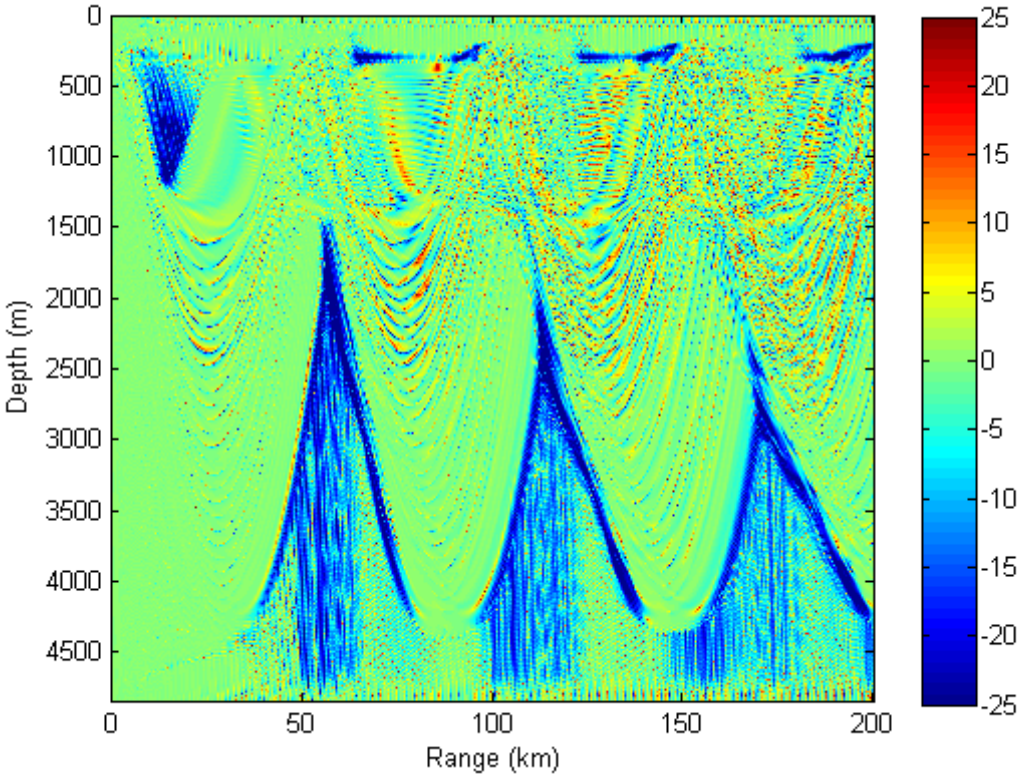

Figure 44. Difference between the Smoothed and Stepped results.

The negative (blue) areas indicate where the stepped profile is greater than the smoothed profile and the positive (red) are indicate the opposite. The areas of greatest differences are evident in the 'shadow zone' (between 500 and 1200m and within 10 to 20km) where the greater acoustic penetration caused by the presence of the steps increases the acoustic energy in this region compared to the smooth profile.

This effect is shown in greater detail by zooming in near this region.

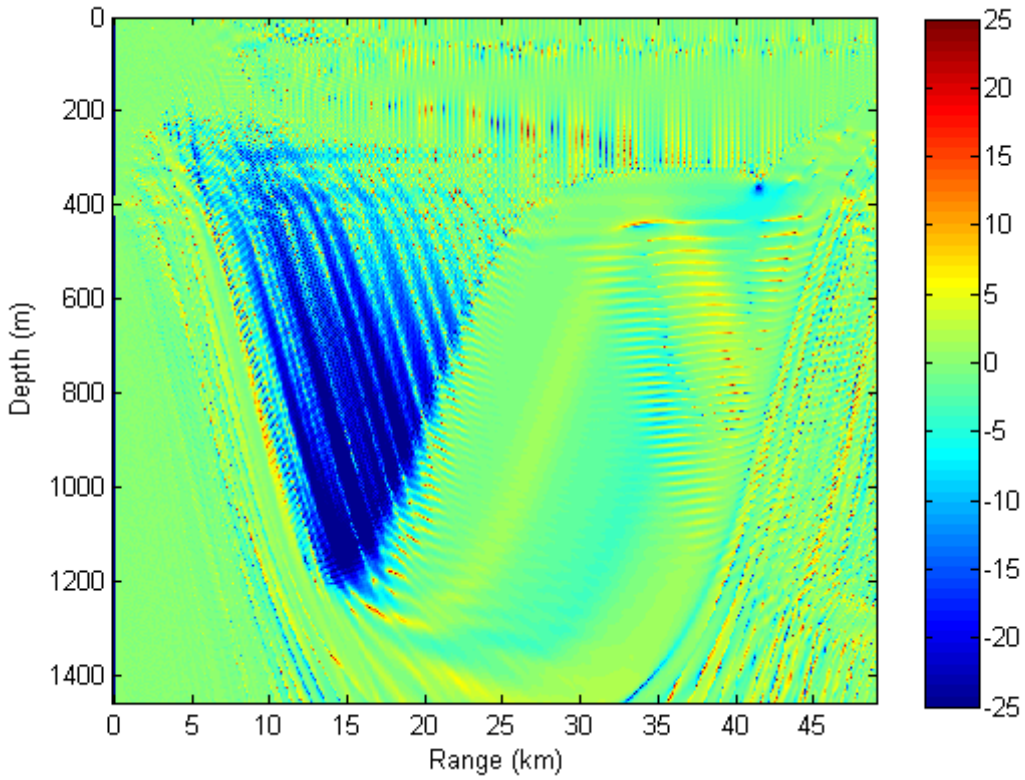

Figure 45. Differences zoomed in.

As shown above there are significant differences (5 to 25dB within ranges of 10 to 25km) between the smooth and stepped profiles that can only be attributed to the presence of the steps. As well as more energy in the shadow zone caused by the steps, there is evidence of more energy (up to 20dB) within the envelope for the smooth profile which reinforces the idea that energy is redistributed from the envelope to the shadow zones by the presence the steps.

The calculations also show that the differences between stepped and no-stepped predictions increase as the range increases; that is the intensity differences accumulate with range.

2. Source Depth 800m

The source depth was then altered to be outside of the staircase region. When the source depth is changed to 800 m (near the sound speed minima at 740m) more acoustic energy is trapped in the sound channel as shown below for the smooth and stepped results.

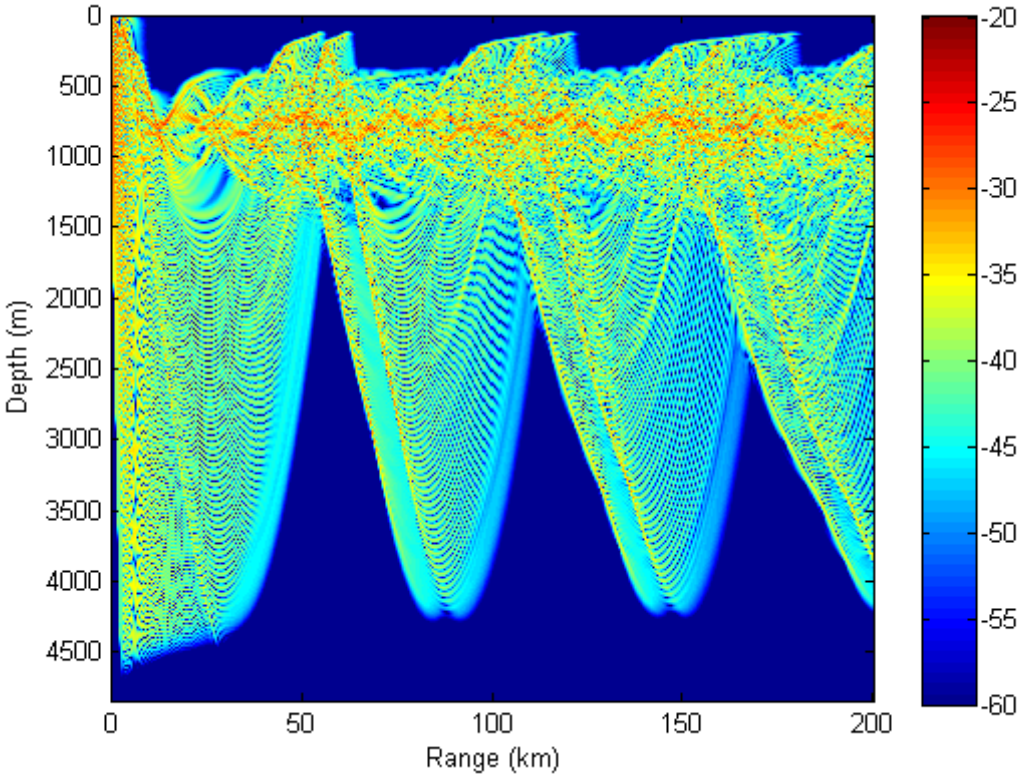

Figure 46. Smooth Source Depth 800m.

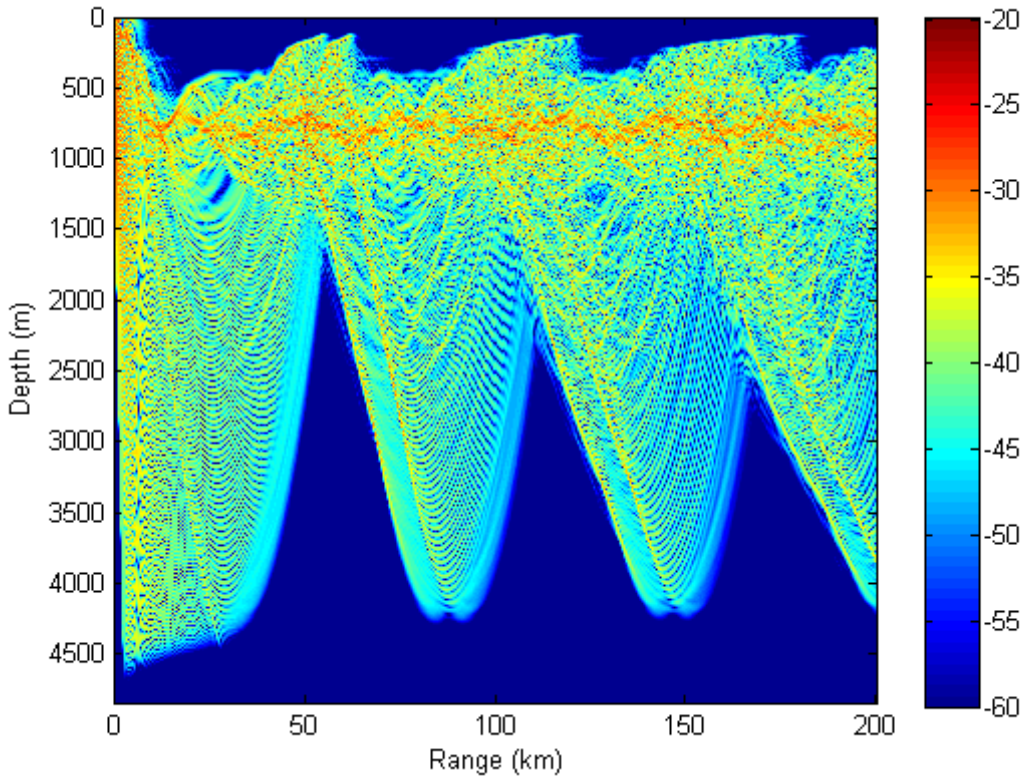

Figure 47. Stepped Source Depth 800m.

Qualitatively the smooth result is again more regular than the stepped result with more acoustic energy evident out of the envelope in the stepped result. The calculated differences are shown below.

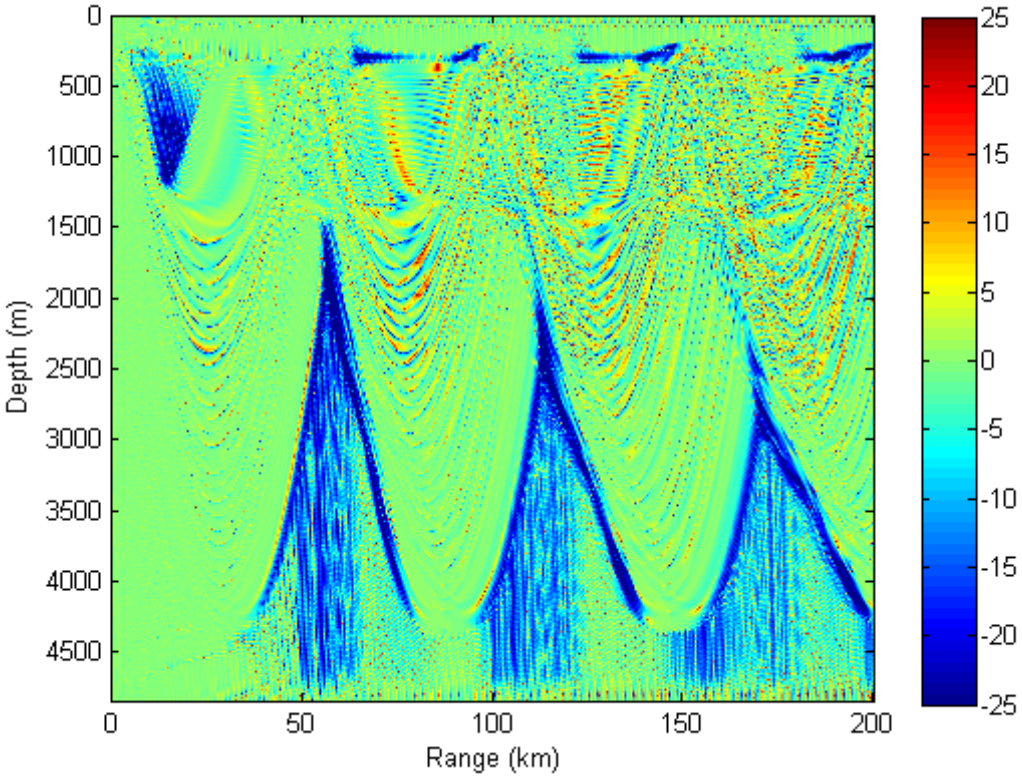

Figure 48. Difference Source Depth 800m.

As before, the blue areas denote where more acoustic energy is evident in the stepped result and red for the smooth result. As shown above there are again significant differences (5 to 25dB within ranges of 10 to 25km) between the smooth and stepped results. With more acoustic energy trapped in the sound channel, the depth of the shadow zone is reduced and this is evident by the smaller area where the stepped result has greater acoustic energy present that the smooth. This is highlighted by zooming in near the source as shown below.

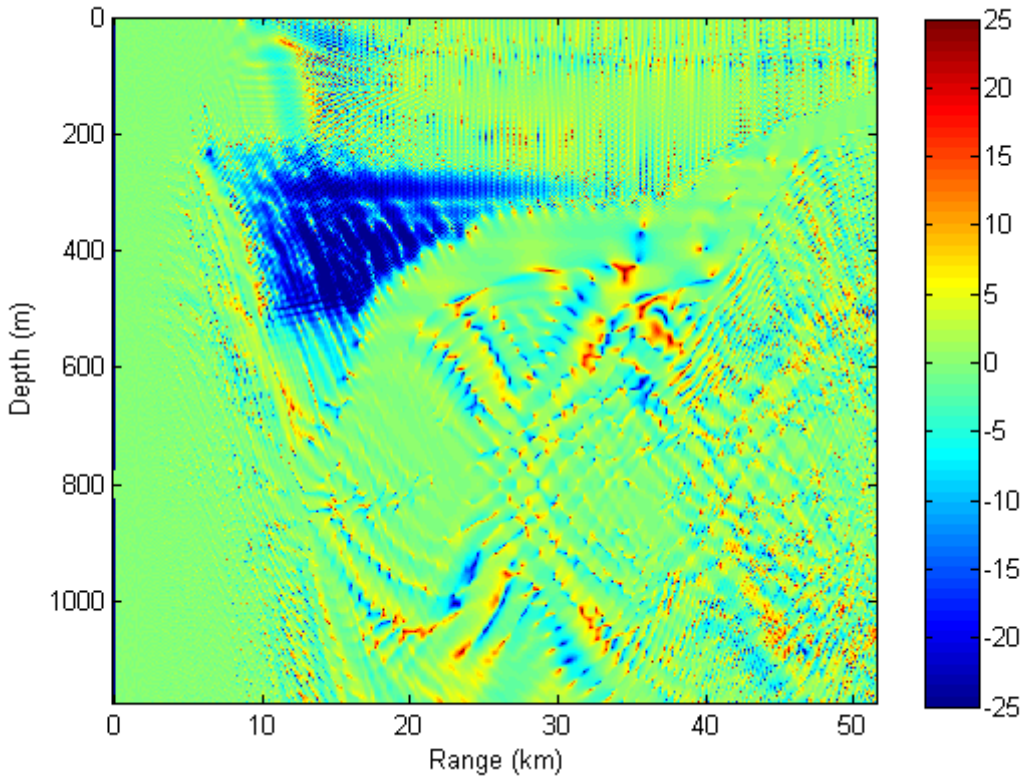

Figure 49. Difference zoomed in.

More acoustic energy for the smooth result has been directed into the sound channel shown by the red areas around the turning points of the envelope in the sound channel.

From these basic results we have an indication that there is a greater effect on the acoustic propagation if the source is located within the staircase region. However, the source and receiver are not necessarily required to be within the staircase region (as observed by Wilson, 2007) for significant differences to be observed.

3. Frequency 1200Hz

Next the model was run using a higher frequency to see if the smaller wavelengths were more susceptible to alterations due to the presence of the staircases. The model was again run with different source depths (400 and 800m) to observe which had the greatest effect. Initially the source depth was set at 800m. As the wavelength was smaller, the parameters for horizontal and vertical resolution were set at 1.25m and 0.33m respectively.

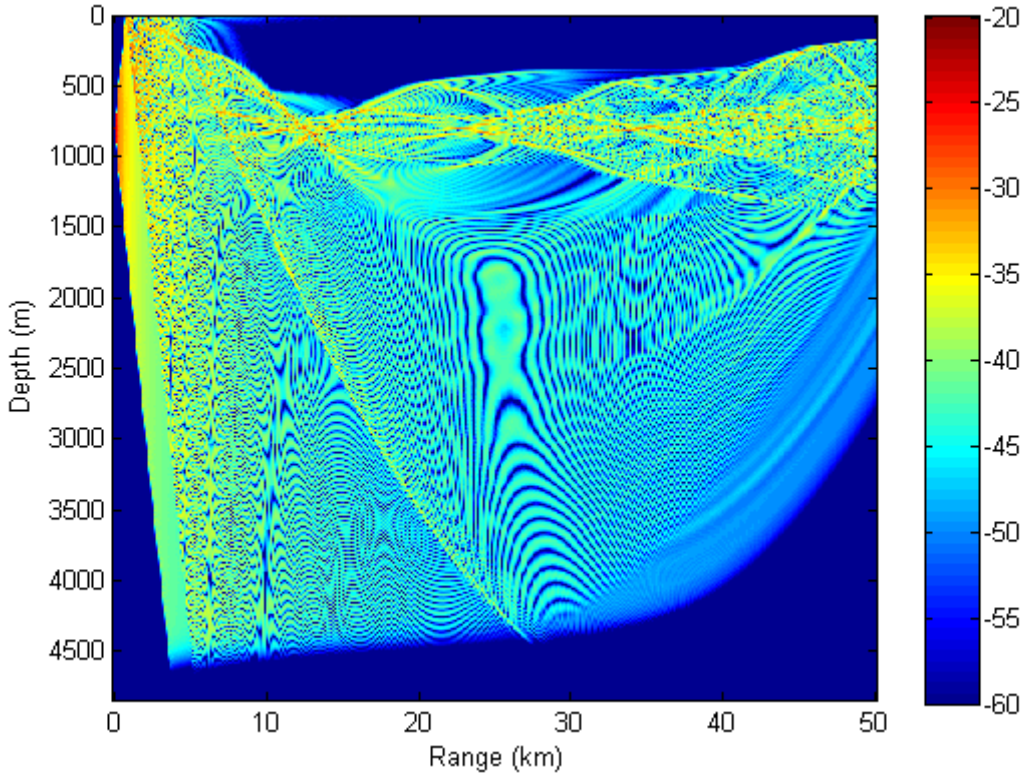

Figure 50. Smoothed Source Depth 800m.

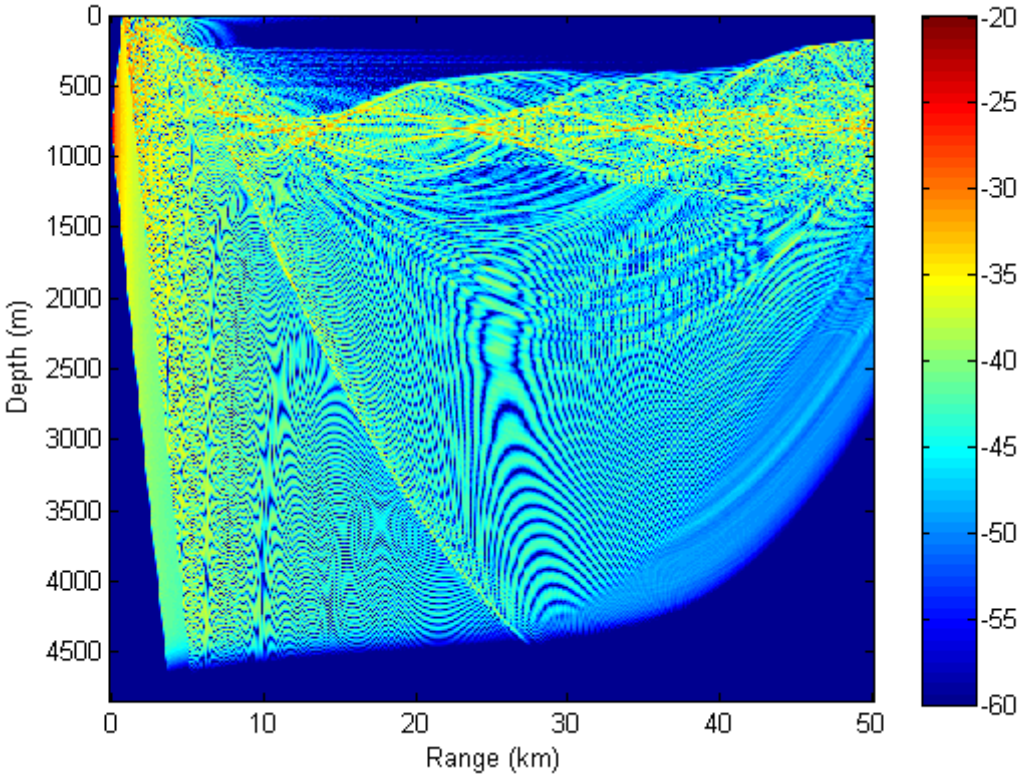

Figure 51. Stepped Source Depth 800m.

Qualitatively, the difference between the two results seems more apparent for this example than the 400Hz case. There is a significant redistribution of acoustic energy from the envelope into the 'shadow zone' from 200 to 500m from around 7 to 15km from the source.

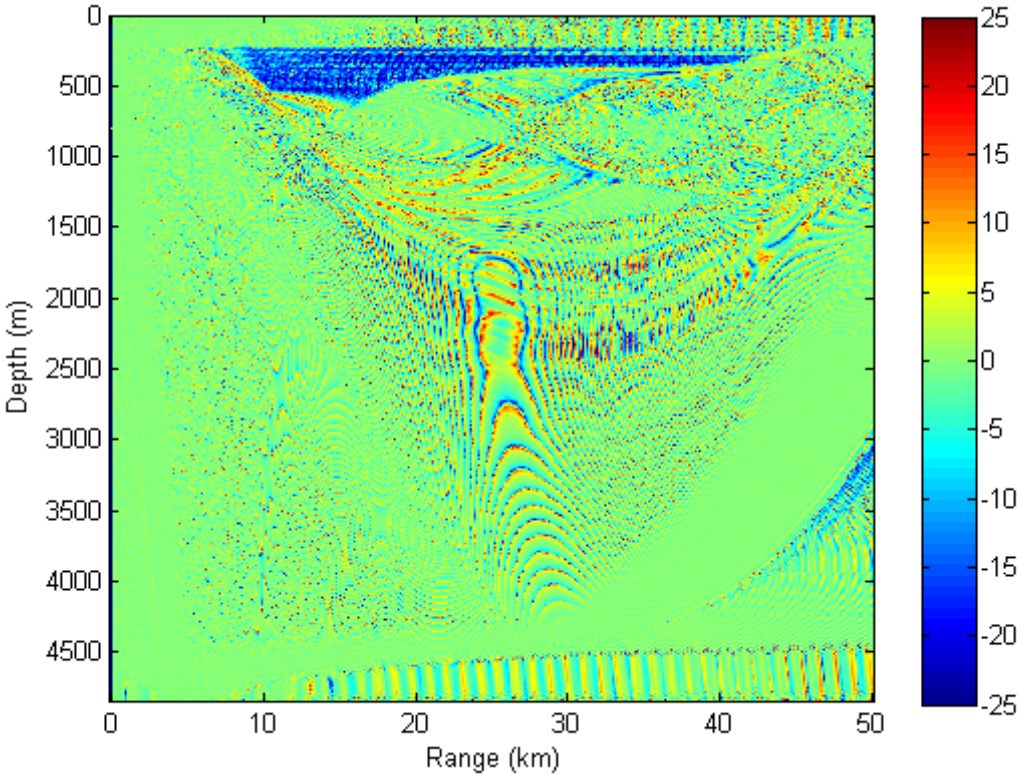

Figure 52. Difference source depth 800m.

The qualitative differences between the results for the two profiles are emphasized in the figure above. As with the previous examples, red areas indicate more acoustic energy for the smoothed result while blue indicates more energy for the stepped. As seen before, there is more energy within the envelope for the smooth result than the stepped and more energy outside the envelope for the stepped result. This is highlighted by zooming in below.

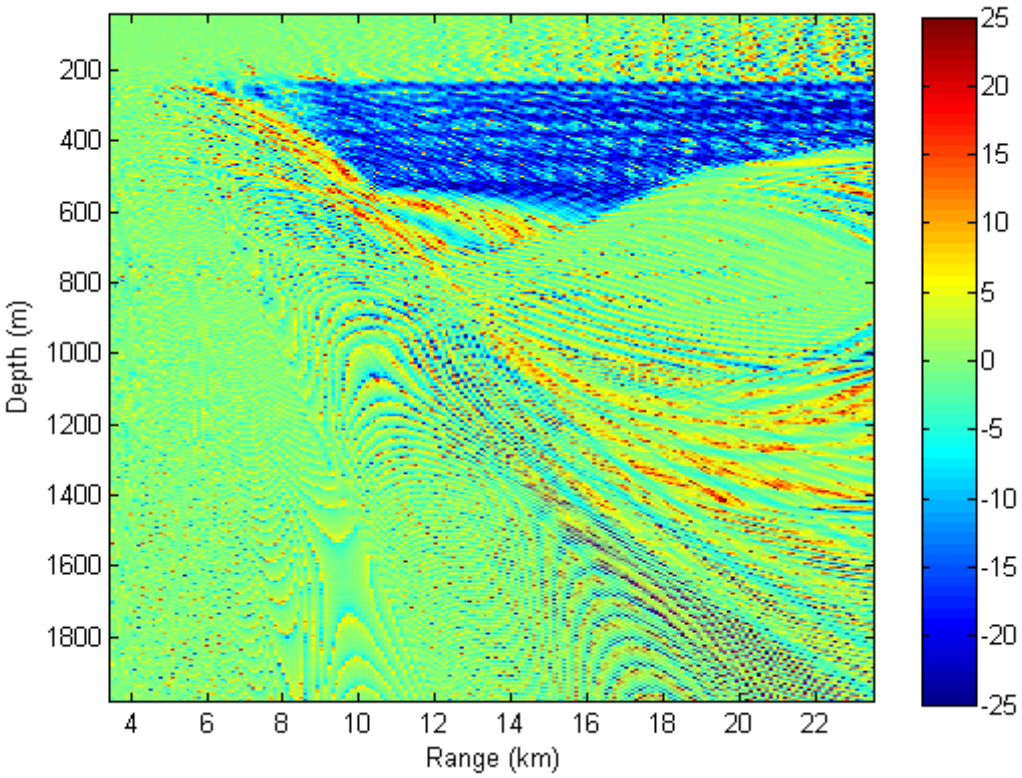

Figure 53. Difference zoomed in.

There is a greater redistribution of energy for this result than the 400Hz which suggest that higher frequencies are more sensitive to the presence of the staircases than lower frequencies.

4. Source Depth 400m

Next we observed when the source depth is 400m (within the staircases). It was proposed that there should be greater differences observed than when the source depth was 800m, as was the cases with the 400Hz example.

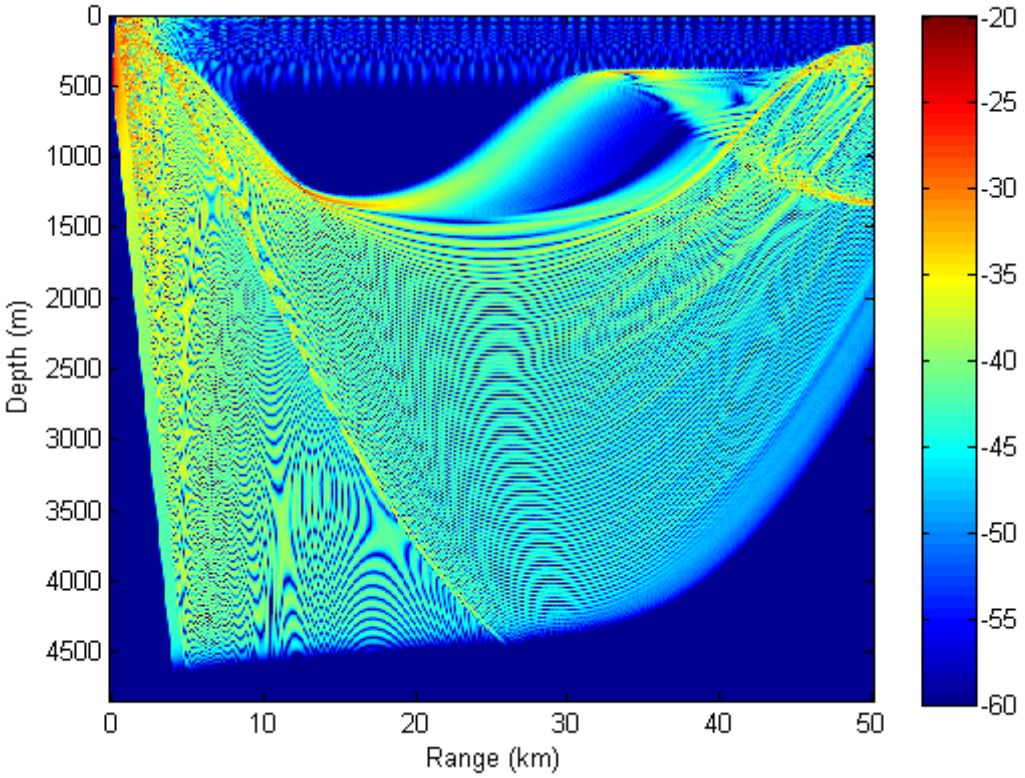

Figure 54. Smoothed Source depth 400m.

The presence of the staircases redistributes more energy out of the envelope than when the source depth was 800m. As with the lower frequency there is less energy directed within the sound channel for the lower source depth.

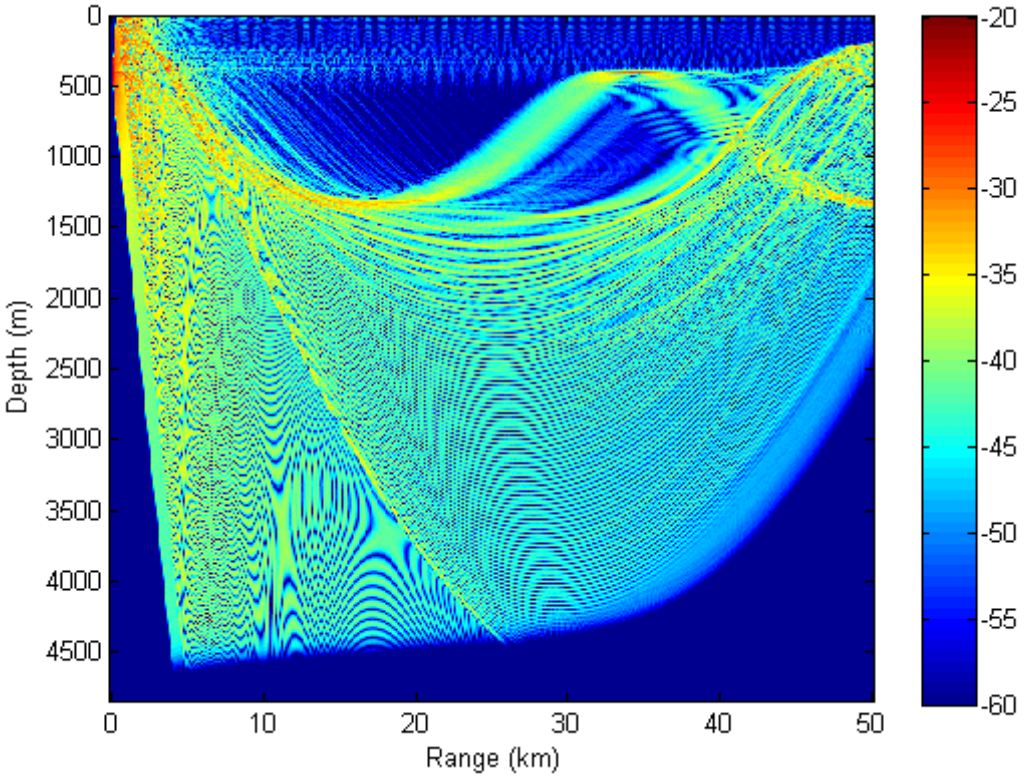

Figure 55. Stepped Sourced Depth 400m.

The stepped result is qualitatively less regular than both the smoothed result at 400m and also the stepped result at 800m. There is a greater amount of acoustic energy evident in the shadow zone and this is emphasized in the calculated differences below.

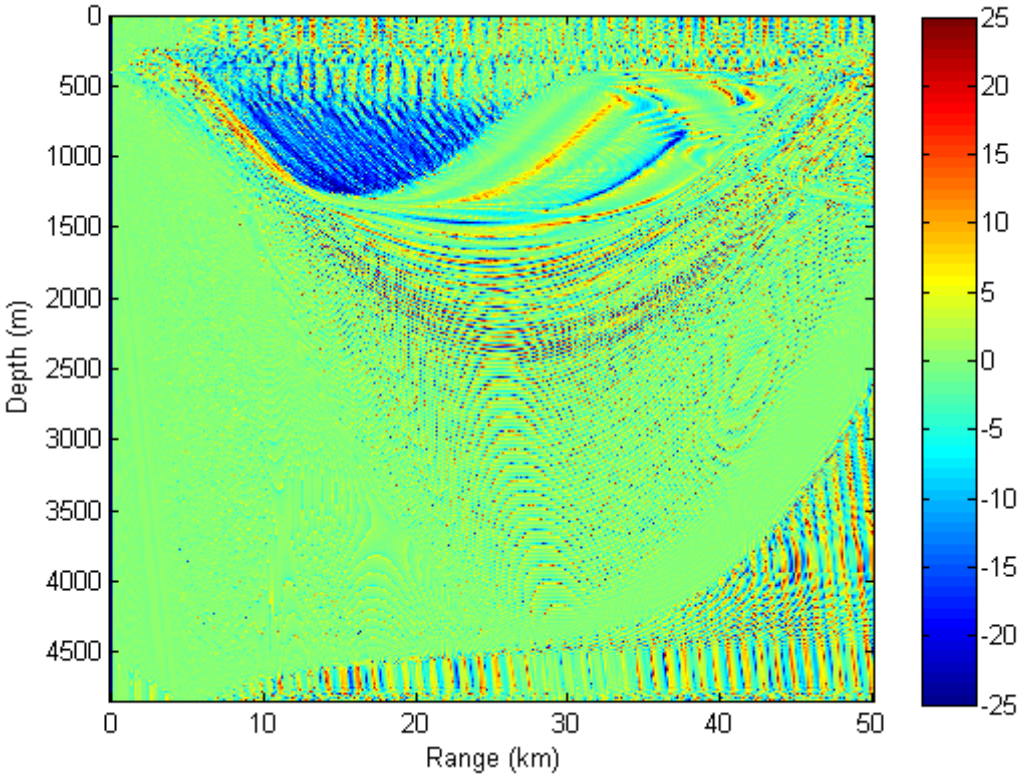

Figure 56. Difference source depth 800m.

There is a much greater redistribution of acoustic energy from the envelope to the shadow zone for this example, as was observed with the 400Hz case. This is again highlighted below by zooming in on the region close to the source.

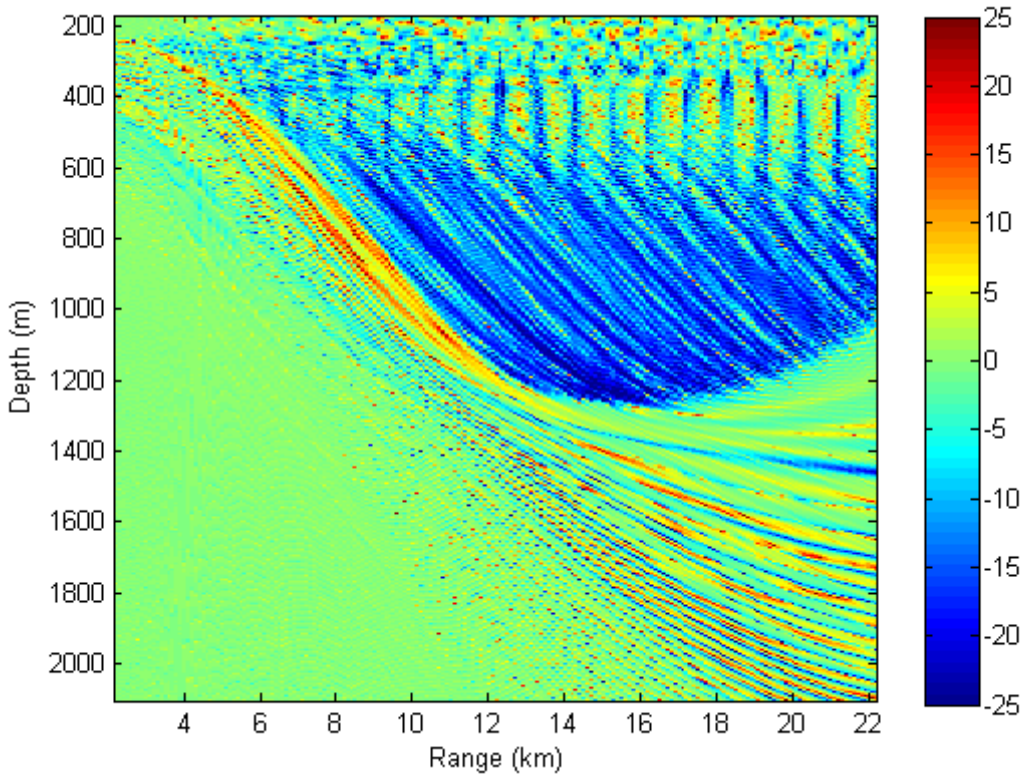

Figure 57. Difference zoomed in.

These four examples indicate that higher frequencies are more affected by the staircases and greater effects are observed when the source is located within the staircases. To further test this idea, the next step is to observe the effects at a lower frequency (50Hz).

5. Frequency 50Hz

Next the model was run for a lower frequency (50Hz) to see if, as Chin-Bing et. al. observed, that the wavelength compatible with the step height is affected more than other frequencies. The average step height is approximately 27m and the wavelength is approximately 30m. Different source

depths (400m and 800m) were used to observe is the source was required to be within the stepped region to have an effect on the acoustic propagation. The parameters for the 400 HZ model runs (horizontal resolution 5m and vertical resolution 1m) were used as the wavelength is larger.

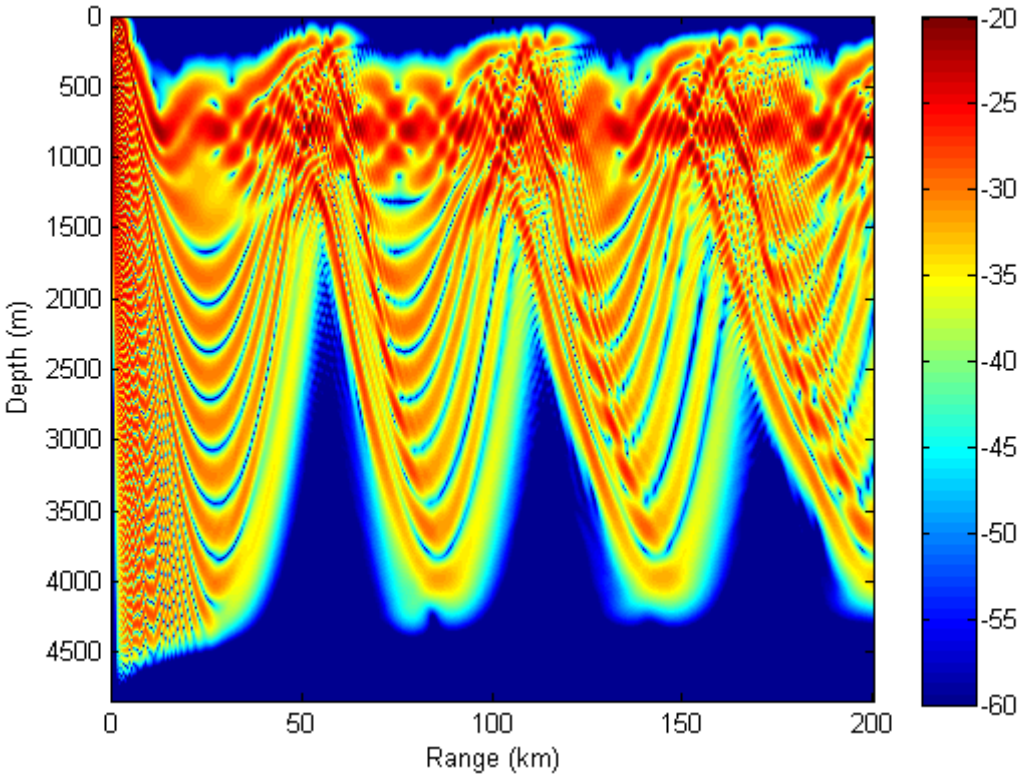

Figure 58. Smoothed source depth 800m

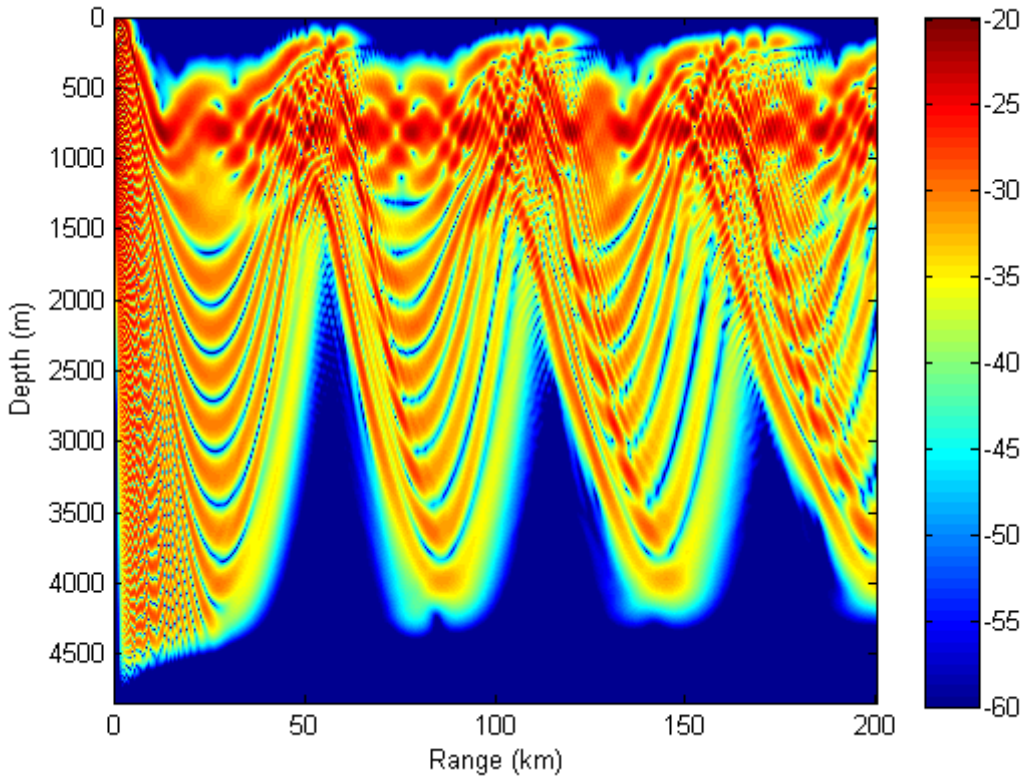

Figure 59. Stepped source depth 800m

Qualitatively the differences are not as obvious as for the higher frequencies. There does not seem to be a significant redistribution of energy from the envelope to the shadow zone as was observed with the higher frequencies. The calculated difference is shown below.

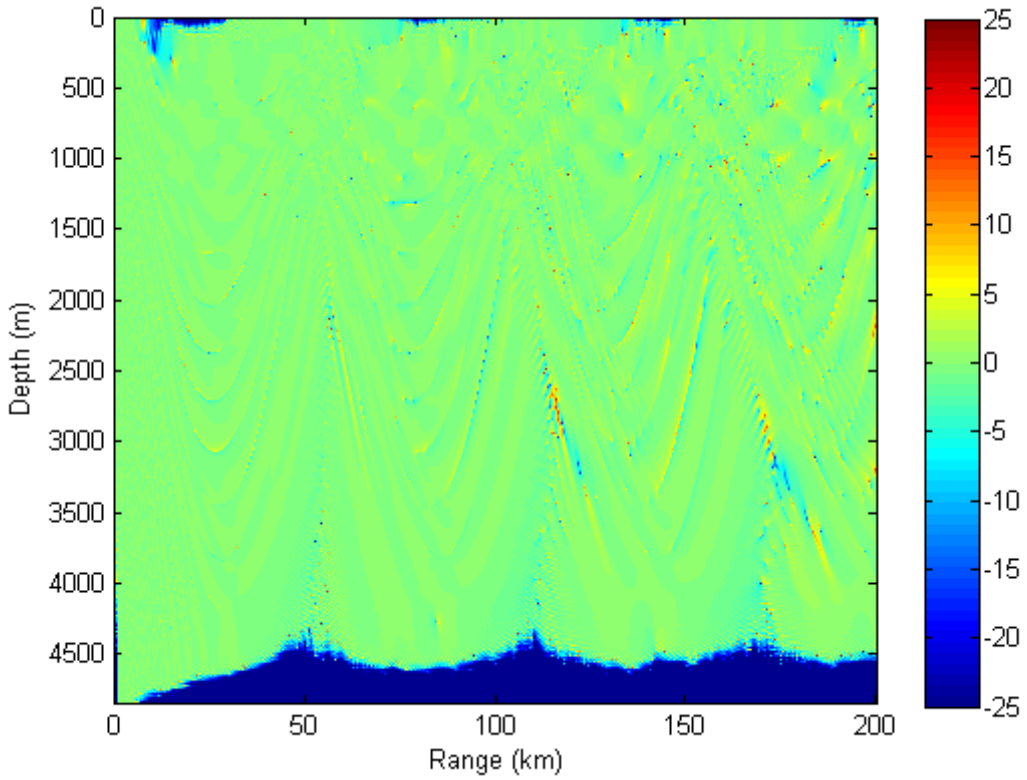

Figure 60. Difference source depth 800m

As before, red areas indicate more energy for the smoothed result and blue for the stepped. The differences are not as great for the lower frequency as the higher frequencies used. The largest differences are near the surface at short ranges or deep at ranges greater than 100km. The differences at close range are highlighted below.

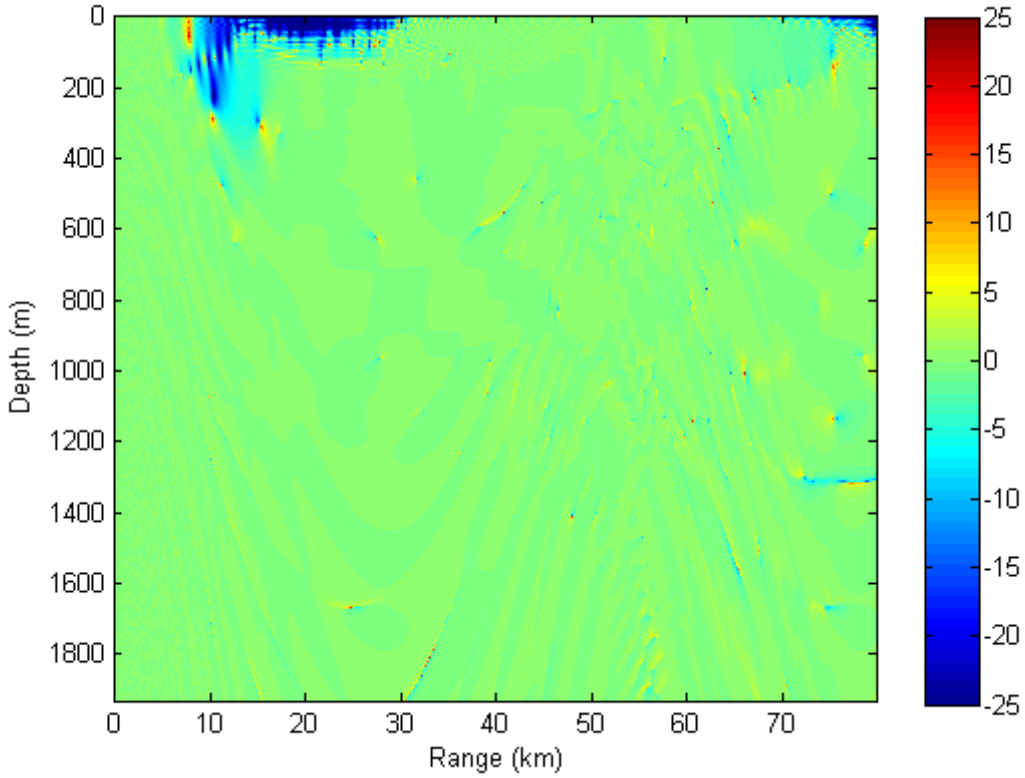

Figure 61. Differences zoomed in

The differences observed are significantly less than observed for both the 400 and 1200Hz examples. This indicates that the lower frequencies are less affected by the presence of the staircases. This is further tested by altering the source depth.

6. Source Depth 400m

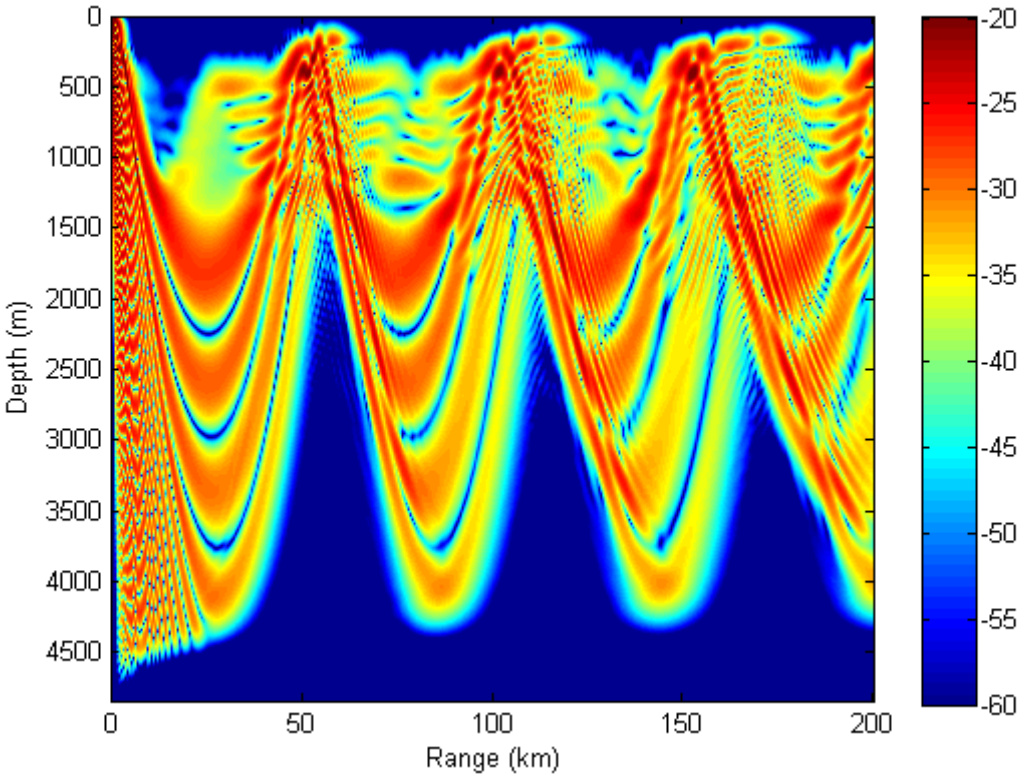

Figure 62. Smoothed source depth 400m

When the source depth is altered to 400m (within the staircases) there is less acoustic energy trapped within the sound channel as was observed when the source depth was 800m. This is consistent with the two other observations at higher frequencies.

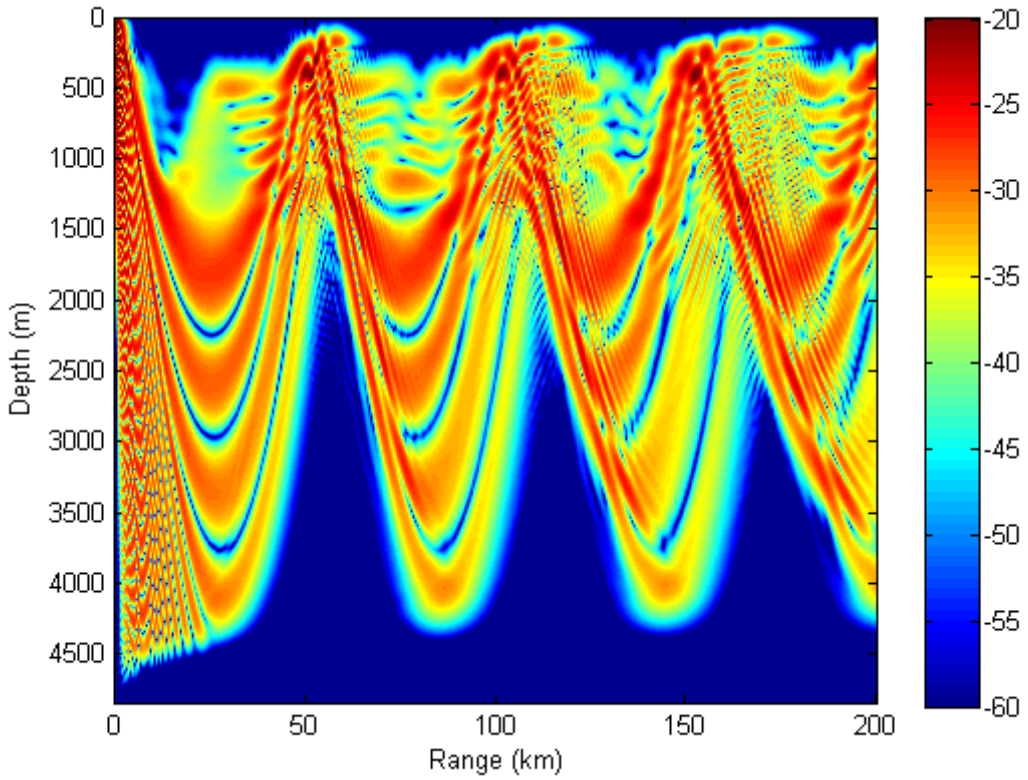

Figure 63. Stepped source depth 400m

Once again, qualitatively the differences at lower frequencies are not as great as higher frequencies. However there seems to be slightly more energy outside the envelope for the stepped result and this is shown below in the calculated differences.

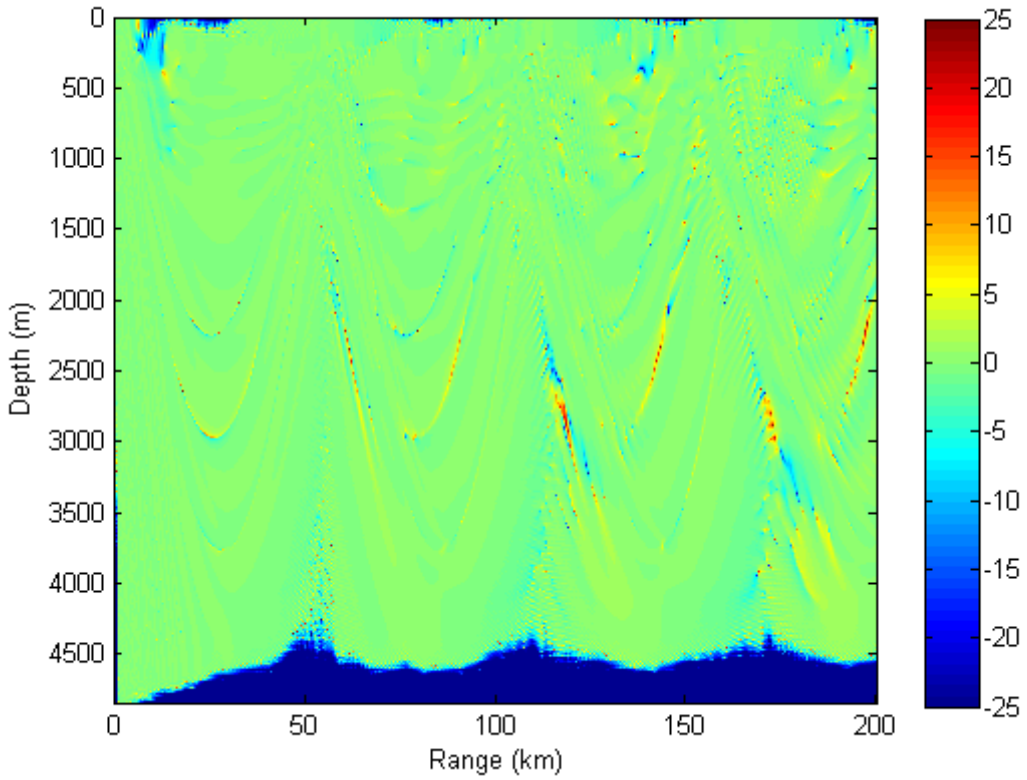

Figure 64. Difference source depth 400m.

The differences for the source depth at 400m are slightly greater than when the source depth was at 800m. This is highlighted by zooming in on the region close to the source below. However, these differences are much smaller than those observed for higher frequencies.

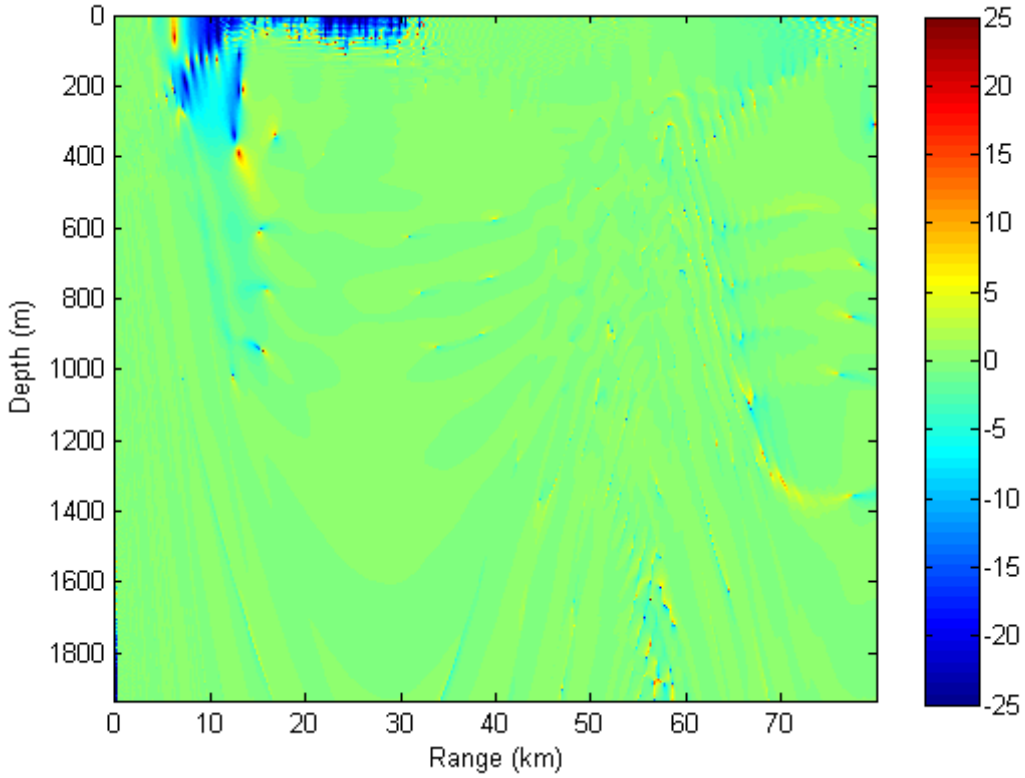

Figure 65. Difference zoomed in

From the model results, the greatest differences were observed for high frequency and when the source depth was within the staircase region.

A notable conclusion from these model results is that the source does not have to be within the staircases for significant effects and that higher frequencies are affected more by the presence of the staircases in this example.

V. CONCLUSIONS

The evidence that thermohaline staircases are a significant feature in ocean mixing is becoming more apparent as we are able to measure and analyze more data to compare what is observed in the ocean with the laboratory.

This study is aimed to clarify three key aspects of staircase dynamics:

i) spatial orientation of interfaces

ii) evolutionary pattern of staircases

iii) acoustic propagation through staircases.

A simple mechanistic model has been developed which predicts the slope of the interfaces and its dependence on the background large-scale T-S distribution.

The preliminary validation of the theory by the C-SALT data is promising and may lead to further developments in determining the three dimensional structure of the staircases.

The merging events noted in the moored profiler data have indicated the prevalence of the instability processes that lead to the B type merger identified in Wilson (2007). Analysis of the growth rates of merging events make it possible to infer the vertical T-S fluxes. We obtain values that are close to fluxes suggested by tracer release experiments. This assists in the verification of the method and also indicates that the fluxes are significant and may account for a significant proportion of the mixing required

for the maintenance of the MOC. Taking into account double-diffusive fluxes should therefore improve the realism of the numerical ocean models.

The acoustic propagation model results indicate that thermohaline staircases have an effect on sound propagation whether inside or out of the staircase region. The effects are more pronounced when the source is located within the staircase region. This is important in evaluating the significance of the features for oceanic and acoustic modeling. Higher frequencies are more affected than lower frequencies. The acoustic model provides information which could be of critical importance for tactic employment in regions susceptible to staircase formation.

LIST OF REFERENCES

Bryan, F. (1987). Parameter sensitivity of primitive equation ocean general circulation models. *J. of Physical Oceanography,* **17**, 970-985.

Chin-Bing, S.A., King, D.B., & Boyd, J.D. (1994). The Effects of Ocean Environmental Variability on Underwater Acoustic Propagation Forecasting. In Robinson, A. & Lee, D., *Oceanography and Acoustics Prediction and Propagation Models* (pp. 24-49). New York: American Institute of Physics.

Clayson, C.A. and Kantha, L.H. (2000). *Small Scale Processes in Geophysical Fluid Flows.* San Diego: Academic Press.

Doherty, K.W., Frye, D.E., Liberatore, S.P. and Toole, J.M. (1999). A moored profiling instrument. *J. of Atmospheric and Oceanic Technology,* **16**, 1816-1829.

Hall, M.M. , Joyce, T.M ., Pickart, R.S ., Smethie Jr, W.M . & Torres, D.J. (2004). Zonal circulation across 52^0W in the North Atlantic. *J. of Geophysical Research,* **109**, C11008, doi:10.1029/2003JC002103.

Jevons, W.S (1857). On the cirrous form of cloud. *London, Edinburgh and Dublin Phil. Mag. And Journal of Science,* 4th Series, **14**, 22-35.

Kelley, D.E. (1988). Explaining effective diffusivities within diffusive oceanic staircases. In J. C. J. Nihoul, & B.M. Jamart (Eds.), *Small-scale turbulence and mixing in the ocean* (pp. 481-502). Amsterdam: Elsevier.

Kunze, E. (2003). A review of oceanic salt-fingering theory. *Progress in Oceanography,* **56**, 399-417.

Ledwell, J.R., Watson, A.J. & Law, C.S. (1993). Evidence for slow mixing across the pycnocline from an open ocean tracer-release experiment. *Nature,* **364**, 701-703.

Merryfield, W.J. (2000). Origin of thermohaline staircases. *J. of Physical Oceanography,* 30, 1046-1068.

Munk, W. (1966). Abyssal recipes. *Deep Sea Research,* **13**, 707-730.

Pacanowski, R.C. and Griffies, S.M. (1999). *The MOM3 Manual.* GDFL Ocean Group Technological Report No. 4, Princeton, NJ: NOAA/Geophysical Fluid Dynamics Laboratory, 680pp.

Radko, T (2003). A mechanism for layer formation in a double diffusive fluid. *J. of Fluid Mechanics,* **497**, 365-380.

Radko, T. (2005). What determines the thickness of layers in a thermohaline staircase? *J. of Fluid Mechanics*, **523**, 79-98.

Radko, T. (2007). Mechanics of merging events for a series of layers in a stratified turbulent fluid. *J. of Fluid* Mechanics, **000**, 1-23.

Radko, T. , Dare, Y. and Kamenkovich, I. (2007). Inferring the pattern of meridional transport from air sea density flux, submitted to *J. of Physical Oceanography.*

Rayleigh, Lord (1883). Investigations of the character of the equilibrium of an incompressible heavy fluid of variable density. *Proc. London Math. Soc.,* **14**, 170-177.

Ruddick, B and Gargett A.E. (2003). Oceanic double diffusion: introduction. *Progress in Oceanography,* **56**, 381-393.

Schmitt, R.W. (1979). The growth rate of super-critical salt fingers. *Deep-Sea Research,* **26A**, 23-40.

Schmitt, R.W., Perkins, H., Boyd, J.D. & Stalcup, M.C. (1987). C-SALT: an investigation of the thermohaline staircases in the western tropical North Atlantic. *Deep-Sea Research,* **34(10)**, 1697-1704.

Schmitt, R.W. (1994). Double diffusion in oceanography. *Annual Review of Fluid Mechanics* **26**, 255–285.

Schmitt, R.W. (2003). Observational and laboratory insights into salt finger convection. *Progress in Oceanography* **56**, 419–433.

Schmitt, R.W , Ledwell, J.R. , Montgomery, E.T. , Polzin, K.L. and Toole, J.M. (2005). Enhanced diapycnal mixing by salt fingers in thermocline of the tropical Atlantic. *Science,* **308**, 5722, 685-688.

Stern, M.E. (1960). The 'salt fountain' and thermohaline convection. *Tellus,* **12**, 172-175.

Stern, M.E. (1969). Collective instability of salt fingers. *J. of Fluid Mechanics,* **35**, 209-218.

Stern, M.E. and Turner, J.S. (1969). Salt fingers and convecting layers. *Deep Sea Research,* **16**, 497-511.

St. Laurent, L. and Schmitt, R.W. (1999). The contribution of Salt Fingers to vertical mixing in the North Atlantic Tracer release Experiment. *J. of Physical Oceanography,* **29**, 1404-1424.

Stommel, H. , Arons, A. B., & Blanchard, D. (1955). An oceanographical curiosity: the perpetual salt fountain. *Deep-Sea Research,* **3**, 152-153.

Stommel, H. (1961). Thermohaline convection with two stable regimes of flow. *Tellus,* **13**,244-260.

Stuebe, D.A. (2005). Temperature and salinity variability in thermohaline staircase layers.

Master of Science in Oceanography and Applied Ocean Science and Engineering Thesis, Woods Hole Oceanographic Institute, Woods Hole, MA.

Tait, R.I. and Howe M.R. (1968). Some observations of thermo-haline stratification in the deep ocean. *Deep Sea Research,* **15**, 275-280.

Toole, J.M., Polzin, R.W. & Schmitt, R.W. (1994). Estimates of diapycnal mixing in the abyssal ocean. *Science,* **264**, 1120-1123.

Turner, J.S. (1965). The coupled turbulent transports of salt and heat across a sharp density interface. *International J. of Heat and Mass Transport*, **8**, 759-767.

Turner, J.S. (1967). Salt fingers across a density interface. *Deep-Sea Research,* **14**, 599-611.

Turner, J.S. (1968). The behavior of a stable salinity gradient heated from below. *J. of Fluid Mechanics,* **33**, 183-200.

Turner, J.S. (1973). *Buoyancy Effects in Fluids.* New York, Cambridge University Press.

Turner, J.S. (1985). Multicomponent convection. *Annual Review of Fluid Mechanics,* **17**, 11-44.

Wilson, A.L. (2007). Structure and Dynamics of the thermohaline staircases in the Beaufort Gyre.

Master of Science in Meteorology and Physical Oceanography Thesis, Naval Postgraduate School,

You, Y. (2002). A global ocean climatological atlas of the Turner angle: Implications for double-diffusion and water-mass structure. *Deep-Sea Research,* 49, 2075-2093.

INITIAL DISTRIBUTION LIST

1. Defense Technical Information Center
   Ft. Belvoir, Virginia

2. Dudley Knox Library
   Naval Postgraduate School
   Monterey, California

3. Directorate of Oceanography and Meteorology
   Royal Australian Navy
   Sydney, NSW, Australia